

Potential of long-term satellite observations and reanalysis products for characterising soil drying: trends and drought events

Martin Hirschi¹, Pietro Stradiotti², Bas Crezee^{1,3}, Wouter Dorigo², Sonia I. Seneviratne¹

¹ETH Zurich, Institute for Atmospheric and Climate Science, Universitätstrasse 16, 8092 Zürich, Switzerland

5 ²TU Wien, Department of Geodesy and Geoinformation, Wiedner Hauptstrasse 8-10, 1040 Vienna, Austria

³now at: Federal Office of Meteorology and Climatology MeteoSwiss, 8058 Zürich-Airport, Switzerland

Correspondence to: Martin Hirschi (martin.hirschi@env.ethz.ch)

Abstract. Soil drying has multiple adverse impacts on environment, society, and economy. It is thus crucial to monitor and
10 characterise related drought events and to understand how underlying geophysical trends may affect them. Here, we compare
the ability of long-term satellite observations and state-of-the-art reanalysis products for characterising soil drying. We
consider the ESA CCI remote-sensing surface soil moisture products (encompassing an ACTIVE, a PASSIVE, and a
COMBINED product) as well as surface and root zone soil moisture from the ERA5, ERA5-Land, and MERRA-2 reanalysis
products. In addition, we use a new root zone soil moisture dataset derived from the ESA CCI COMBINED product.

15

We analyse global surface and root zone soil moisture trends in these products over the 2000–2022 period. Furthermore, we
investigate the impact of the products' trend representation on their ability to capture major seasonal soil moisture (or
agroecological) drought events as a use case. The latter is based on the analysis of 17 selected drought events documented in
scientific literature, which are characterised by their severity (the time-accumulated standardised soil moisture anomalies),
20 magnitude (the minimum of the standardised anomalies over time), duration, and spatial extent.

The soil moisture trends are globally diverse and partly contradictory between products. ERA5, ERA5-Land and
ESA CCI COMBINED show larger fractions of drying trends, ESA CCI ACTIVE and MERRA-2 more widespread wetting
trends. The differences between reanalysis products are related to a positive mean bias in the precipitation trends and
25 regionally negative biases in surface air temperature trends of MERRA-2 compared to ground observational products, which
suggests that this reanalysis underestimates drying trends. Given these biases in the MERRA-2 precipitation and temperature
trends, but also considering available validation studies, the ESA CCI COMBINED-based products and ERA5-Land are
considered more reliable and are consecutively used for a synthesis of global surface and root zone soil moisture trends. This
synthesis suggests a consistent tendency towards soil drying during the last two decades in these products in 49.3% of the
30 surface and 44.5% of the root zone layers of the covered global land area. The respective fractions of wetting trends amount
to 21.1% and 20.6% for surface and root zone respectively, and areas with no trend direction consensus to 29.6% and 35.0%
respectively, reflecting the considerable uncertainties associated with global soil moisture trends. Geographically, the drying

is localized in parts of Europe and the Mediterranean, in the region of the Black Sea/Caspian Sea and Central Asia, in Siberia, in parts of western USA and the Canadian Prairies, as well as larger parts of South America, parts of southern and northern Africa and northwest Australia.

All investigated products mostly capture the considered drought events. Overall, the events tend to be least pronounced in the ACTIVE remote-sensing product across all drought metrics, particularly in the magnitudes. Also, MERRA-2 shows lower drought magnitudes than the other products both in the surface layer and the root zone. The COMBINED remote-sensing products (surface and root zone soil moisture dataset) display partly stronger drought severities than the other products. In the root zone, the droughts are dampened in magnitude and smaller in spatial extent than in the surface layer, but show a tendency to prolonged durations and stronger severities. The product differences in magnitude and severity of the drought events are consistent with the differences in soil moisture trends, which demonstrates that the representation of soil moisture trends plays a fundamental role for the drought-detection capacity of the different products.

1 Introduction

Soil drying and related droughts have multiple impacts on environment, society, and economy, including substantial impacts on agriculture, ecosystems, and public water supply (Stahl et al., 2016; Seneviratne et al., 2021). Furthermore, both can act as triggers for other natural hazards at the sub-continental scale, including increased wildfire activity (Gudmundsson et al., 2014). Through feedback with the atmosphere, the prevailing dry conditions may further enhance air temperatures and trigger heat extremes (e.g., Miralles et al., 2014; Hirschi et al., 2011; Mueller and Seneviratne, 2012).

Based on varying data products, regional soil moisture drying trends have been reported, e.g., for East Asia (e.g., Jia et al., 2018; Cheng et al., 2015), Western and Central Europe (e.g., Trnka et al., 2015; Scherrer et al., 2022), and the Mediterranean (e.g., Hanel et al., 2018; Moravec et al., 2019). Also, global studies have documented soil moisture drying during past decades for several regions (Dorigo et al., 2012; Albergel et al., 2013; Gu et al., 2019; Preimesberger et al., 2021). However, the involved products show considerable differences in the global patterns and magnitudes of the soil moisture drying. At the same time, important drought metrics, such as duration and magnitude, rely on the robustness of the applied climatology (Lloyd-Hughes and Saunders, 2002), as demonstrated by the relevance of the baseline period as design choice in drought studies (Champagne et al., 2019). Any inherent trend in the climatology will result in a different distribution of the data, potentially affecting the ranking of drought events or even their detection. However, the impact of soil drying and its uncertainty on drought representation is understudied.

The recent IPCC AR6 report assessed three types of droughts (Seneviratne et al., 2021; Douville et al., 2021): meteorological droughts based on precipitation deficits, agricultural and ecological droughts – here referred to as “agroecological droughts”

65 (Zaitchik et al., 2023) – related to deficits in soil moisture and other measures of changes in the land water balance, and hydrological droughts related to streamflow deficits. The most impact-relevant drought types are agroecological and hydrological droughts. The primary driver of these droughts is a lack of precipitation (meteorological drought; see e.g., Seneviratne, 2012; Seneviratne et al., 2021; Liu et al., 2020). Increased evapotranspiration due to enhanced radiation, wind speed, or vapor pressure deficit (itself linked to temperature and relative humidity) can further intensify the water shortage and lead to critical soil moisture values (agroecological drought) inducing e.g., adverse impacts on vegetation development (due to increased water stress) and crop yield reduction/failure (e.g., Teuling et al., 2013; Seneviratne et al., 2021; Bueechi et al., 2023). Furthermore, pre-conditioning (pre-event soil moisture, surface, snow and/or groundwater storage) can contribute to the emergence of agroecological and hydrological droughts (Koster et al., 2010). Under strong droughts, soil moisture can also become limiting for evapotranspiration, thus reducing the evaporative cooling effect (e.g., Miralles et al., 2014; Seneviratne et al., 2010). The IPCC AR6 report concluded that a number of regions of the world are affected by increases in agroecological droughts (Seneviratne et al., 2021), mostly due to increases in evapotranspiration (Padron et al., 2020). Thus, monitoring and characterising soil moisture droughts is crucial, and will become more important with ongoing global warming.

80 Since in situ observations of soil moisture are still scarce and not continuously available in space and time over long time periods (Dorigo et al., 2011; Dorigo et al., 2021b), reanalysis and merged remote-sensing products provide an alternative for global long-term timeseries to investigate drying trends and soil moisture droughts on supra-regional scales. Here, we investigate the ability of the long-term remote-sensing dataset ESA CCI soil moisture (encompassing multi-sensor merged ACTIVE, PASSIVE and COMBINED surface soil moisture products, as well as a new root zone soil moisture product based on COMBINED) and selected state-of-the-art reanalysis products (ERA5, the offline ERA5-Land, and MERRA-2) for characterising soil drying. Soil moisture trends in long-term satellite observations and differences in these trends between measuring approaches are still understudied. Most of the available ESA CCI soil moisture based trend analyses use the COMBINED product (e.g., Dorigo et al., 2012; Albergel et al., 2013; Feng and Zhang, 2015; Gu et al., 2019; Preimesberger et al., 2021) and many focus on regional trends only (e.g., Li et al., 2015; Rahmani et al., 2016; Wang et al., 2016; Zheng et al., 2016; An et al., 2016; Jia et al., 2018). Previous analyses indicated that global trend patterns of ESA CCI COMBINED soil moisture may be subject to differences between product versions (Hirschi et al., 2023), due to yet unknown reasons. Even though the patterns have become more stable with latest product versions, potential sources of uncertainty include the different merging steps involved in the ESA CCI processing chain, changes in the sensor composition between versions, and characteristics of the underlying ACTIVE and PASSIVE products per se that translate into the COMBINED product.

95 Understanding where confidence in the remote-sensing based soil moisture trends is justified, and where not, is thus fundamental for the use of such products as climate data record. The same applies to (land) reanalysis products, which we use as a comparison. To attribute some of the product differences, potential drivers of the global soil moisture trends in the reanalyses are analysed by considering trends in relevant variables of the land water balance and surface air temperature, and

100 corresponding trends in ground observational data. Additionally, we look at bioclimatic indicators and land-surface characteristics that potentially affect the stability of the soil moisture retrieval and the reanalysis-based soil moisture.

105 Focussing on agroecological drought as a use case, we further systematically characterise documented major seasonal drought events in the 2000–2022 period and analyse the impact of the soil moisture trend representation of the products on their ability to capture these events. The drought events are selected based on scientific literature and drought reports, providing the temporal and spatial bounds for the analysis. Given the lack of widely available ground data of soil moisture, we rely on well documented drought events and focus on the relative behaviour of the products within the temporal and spatial bounds of the events. Thus, we do not aim for a in situ validation of the products regarding their representation of the soil moisture trends and considered drought events but focus instead on the product ensemble to identify the products with larger deviations from the majority and collect convergence of evidence. The considered products, in particular the ones from the Copernicus Climate Data Store (CDS), also offer new opportunities for monitoring of ongoing droughts and applications like drought index insurances (Vroege et al., 2021), since they are available in near real-time.

2 Data

2.1 Remote sensing and reanalysis soil moisture

115 Soil moisture from both the near-surface soil layer as well as the root zone is considered. Despite the overall strong correlation of surface soil moisture with deeper soil layers, evapotranspiration and vegetation processes might be more sensitive to variations of root zone soil moisture, in particular under very dry conditions (Hirschi et al., 2014). The surface layer corresponds to roughly 0–5 cm depth (according to GCOS, 2016) and covers the penetration depth of microwave remote sensing soil moisture products. Note that this upper soil layer depth may slightly vary per product depending on the microwave sensing frequency or the land-surface model. For the root zone, the soil layer of 0–100 cm depth is considered. 120 All data presented in the following has been re-gridded to a common $0.5^\circ \times 0.5^\circ$ spatial resolution using first order conservative remapping from the Climate Data Operators (CDO) after the retrieval.

2.1.1 ESA CCI soil moisture

125 The European Space Agency (ESA) Climate Change Initiative (CCI) soil moisture (ESA CCI soil moisture, v08.1) provides satellite-retrieved surface soil moisture over the globe from a large set of active and passive microwave sensors (with soil penetration depths of $\sim 2\text{--}5$ cm). The dataset contains the following sub-products: "ACTIVE", "PASSIVE" and "COMBINED" (denoted ESA-CCI-ACT, ESA-CCI-PAS and ESA-CCI-COM in the following). The ESA-CCI-ACT and ESA-CCI-PAS products were created by using scatterometer (active microwave sensing) and radiometer (passive microwave sensing) soil moisture products, respectively. For ESA-CCI-COM, all active and passive single-sensor products are directly merged based on the signal-to-noise ratio of the input datasets (Gruber et al., 2019). Note that in the merging process for

130 ESA-CCI-COM, the active and passive L2 products are scaled against surface soil moisture from the GLDAS-Noah v2.1 land surface model (Rodell et al., 2004) from which the dynamic range is inherited (Dorigo et al., 2017; Gruber et al., 2019). As of v08.1, a break-adjustment is implemented for ESA-CCI-COM, which corrects for breaks in mean and variance (Preimesberger et al., 2021; Su et al., 2016).

135 Microwave retrievals are impossible under snow and ice or when the soil is frozen, and complex topography, surface water, and urban structures have negative impacts on the retrieval quality (Dorigo et al., 2017; Dorigo et al., 2015). In addition, dense vegetation attenuates the microwave emission and backscatter from the soil surface and may (partly) mask the soil moisture signal. Altogether, these limitations result in spatial and temporal data gaps of remote sensing-based soil moisture estimates, with main affected areas in the high latitudes during winter and the tropical rainforests with very dense vegetation.

140

The product is provided on a $0.25^\circ \times 0.25^\circ$ spatial grid and in daily temporal resolution from November 1978 onwards (in case of ESA-CCI-PAS and ESA-CCI-COM) or from August 1991 onwards, respectively (in case of ESA-CCI-ACT), and data is available until 2022. Data coverage is limited in the early years of ESA-CCI-COM (and -PAS) when only few passive sensors are available (e.g., Loew et al., 2013). The inclusion of active sensors from July 1991 (Gruber et al., 2019) and the
145 availability of multiple passive and active sensors after 2000 increased the spatio-temporal coverage (Hirschi et al., 2023). The ESA CCI soil moisture product has been extensively validated (Dorigo et al., 2015; Beck et al., 2021; Hirschi et al., 2023) and used in various research applications (see Dorigo et al., 2017 for an overview).

In addition to these ESA CCI surface soil moisture products, an ESA-CCI-COM-based root zone soil moisture dataset is
150 included in the analysis, which is derived by extrapolating surface soil moisture to deeper soil layers (denoted ESA-CCI-COM-RZSM). The extrapolation is based on an exponential filter (Wagner et al., 1999; Albergel et al., 2008), which is applied to ESA-CCI-COM soil moisture (v08.1) and uses optimal values for the temporal length of the filter (T-parameter) determined from a large number of in situ time series (Pasik et al., 2023). The data represents the root zone down to one meter soil depth and will be released with the ESA CCI soil moisture products as of v09.1.

155 **2.1.2 ERA5**

ERA5 is the fifth generation ECMWF reanalysis of the global climate and weather for the past decades (Hersbach et al., 2020). Data is available from 1940 onwards until present and updated daily with a latency of about 5 days. ERA5 is produced using 4D-Var data assimilation in CY41R2 of ECMWF's Integrated Forecast System (IFS). ERA5 provides hourly data with a spatial resolution of 31 km.

160

The land-surface scheme of ERA5, HTESSSEL (Hydrology-Tiled ECMWF Scheme for Surface Exchanges over Land, Balsamo et al., 2009) distinguishes between four different soil layers with the following layer depths: layer 1 at 0–7 cm;

layer 2 at 7–28 cm; layer 3 at 28–100 cm; and layer 4 at 100–289 cm. Apart from the assimilation of 2 m temperature and relative humidity pseudo-observations (e.g., De Rosnay et al., 2013), ERA5 is the first ECMWF reanalysis that includes
165 remotely-sensed observations in a soil moisture analysis. Remote-sensing soil moisture from scatterometers (ERS-1, -2; MetOp-A, -B ASCAT) are assimilated in the land data assimilation from 1991 onward using a Simplified Extended Kalman Filter for the three soil moisture layers of the top first meter of the soil (Hersbach et al., 2020; De Rosnay et al., 2014).

On the one hand, we focus on layer 1 (0–7 cm), i.e., (near-)surface soil moisture to allow comparison with the ESA CCI
170 remote sensing soil moisture products (see above). On the other hand, average soil moisture from layers 1–3 (i.e., 0–100 cm; layer-depth weighted) is considered as a representation of root zone soil moisture. The ERA5 data has been retrieved on a regular latitude/longitude grid of $0.25^\circ \times 0.25^\circ$ spatial resolution and hourly temporal resolution from the CDS. We have further aggregated the retrieved hourly data to daily means.

2.1.3 ERA5-Land

175 The land component of the ERA5 reanalysis provides global, hourly, high-resolution information of the water and energy cycles over land in a consistent representation (Muñoz-Sabater et al., 2021). ERA5-Land is a single simulation based on the land-surface model HTESSEL (Balsamo et al., 2009) forced by ERA5 near-surface atmospheric fields, with additional lapse-rate correction of temperature. Compared to ERA5, near-surface quantities are available in higher spatial resolution, and the soil parameters are more homogeneous between ERA5 production streams (Hersbach et al., 2020). There is no feedback
180 from the land surface model to the atmospheric parameters, and atmospheric observations only influence the land surface simulations indirectly through the ERA5 forcing. Unlike ERA5, ERA5-Land does not assimilate remote sensing soil moisture or other land variables. ERA5-Land is available from 1950 onwards and updated monthly with a latency of about three months. It provides hourly data with a spatial resolution of 9 km, thus allowing more spatial detail compared to ERA5.

185 The representation of the soil compartments in ERA5-Land is consistent with ERA5 since both products consider the same land-surface model HTESSEL (see Sect. 2.1.2). Consequently, as for ERA5, soil moisture from layer 1 (surface soil moisture) and from layers 1–3 (root zone soil moisture, layer-depth weighted average) are considered in the analyses. Evaluation against in situ observations and other reference datasets shows the added value of ERA5-Land in the description of the hydrological cycle when compared to ERA5, with enhanced soil moisture and lake representation, and better
190 agreement of river discharge with observations (Muñoz-Sabater et al., 2021).

The ERA5-Land data has been extracted on a regular latitude/longitude grid of $0.25^\circ \times 0.25^\circ$ spatial resolution and hourly temporal resolution from the CDS. We have further aggregated the retrieved hourly data to daily means.

2.1.4 MERRA-2

195 The Modern-Era Retrospective Analysis for Research and Applications, version 2 (MERRA-2), is the latest atmospheric
reanalysis of the modern satellite era produced by NASA's Global Modeling and Assimilation Office (GMAO; Gelaro et al.,
2017). It was introduced to replace the original MERRA dataset because of the advances made in the assimilation system
that enables assimilation of modern hyperspectral radiance and microwave observations, along with GPS-Radio Occultation
200 datasets. Among the advances in MERRA-2 are the assimilation of aerosol observations, several improvements to the
representation of the stratosphere including ozone, and improved representations of cryospheric processes. Other
improvements in the quality of MERRA-2 compared with MERRA include the reduction of some spurious trends and breaks
related to changes in the observing system and reduced biases and imbalances in aspects of the water cycle. MERRA-2
provides data beginning in 1980, at $0.625^\circ \times 0.5^\circ$ spatial resolution and hourly temporal resolution. For an overview of the
dataset, see Gelaro et al. (2017).

205

The land surface model used in MERRA-2 is the Catchment model (CLSM; Koster et al., 2000). It explicitly addresses
subgrid-scale soil moisture variability and its effect on runoff and evaporation, using the basic computational element of a
hydrological catchment. The land hydrology of MERRA-2 has been assessed against GRACE terrestrial water storage data
as well as against in situ soil moisture data (Reichle et al., 2017b). MERRA-2 is produced using four separate streams,
210 initialised in 1979, 1991, 2000, and 2010. The first year of each stream is designated as spinup (Bosilovich et al., 2015). The
land surface restart files for each MERRA-2 stream were themselves spun up for at least 20 years, using the offline (land
only) version of the MERRA-2 land model forced with MERRA surface meteorological fields (Reichle et al., 2017a).
Despite this allowance for a spinup, it has been documented that discontinuities remain in the high latitudes for root zone soil
moisture (cf. Fig. 13 of Reichle et al., 2017a).

215

The variables SFMC (water surface layer, 0–5 cm depth) and RZMC (water root zone, 0–100 cm depth) have been retrieved
from the Goddard Earth Sciences Data and Information Services Center (GES DISC) as daily aggregated data (GMAO,
2015).

220

Table 1 Product summary of the considered soil moisture products. The column ‘horizontal grid spacing’ lists the resolution of the data retrieved, if applicable the native resolution of the dataset is listed in brackets. Similarly, for ‘temporal resolution’, values between brackets indicate the underlying temporal resolution when this differs from the retrieved resolution.

Dataset	Institution	Type of product	Time range	Horizontal grid spacing	Soil layer depth	Variable name	Temporal resolution	Main reference
ESA-CCI-COM/-ACT/-PAS v08.1	ESA	Active and passive microwave remote sensing	Nov 1978 / Aug 1991–2022	0.25°x0.25°	~2–5 cm	sm	Daily	Gruber et al. (2019); Dorigo et al. (2017); Dorigo et al. (2023)
ESA-CCI-COM-RZSM v08.1	TU Wien	Exponential filter-based root zone soil moisture	2000–2022	0.25°x0.25°	0–100 cm	rzsm_1m	Daily	Pasik et al. (2023)
ERA5	ECMWF	Atmospheric reanalysis	1940–present	0.25°x0.25° (~31 km)	0–7 cm, 0–100 cm	swv11, swv11–3	Hourly	Hersbach et al. (2020)
ERA5-Land	ECMWF	Land-surface reanalysis	1950–present	0.25°x0.25° (~9 km)	0–7 cm, 0–100 cm	swv11, swv11–3	Hourly	Muñoz-Sabater et al. (2021)
MERRA-2	NASA	Atmospheric reanalysis	1980–present	0.625°x0.5°	0–5 cm, 0–100 cm	SFMC, RZMC	Daily (hourly)	Bosilovich et al. (2015)

225 2.2 Other meteorological variables from reanalyses and ground observations

Apart from soil moisture, the following variables are used from the ERA5, ERA5-Land and MERRA-2 reanalysis products: total precipitation, evapotranspiration, runoff and surface air temperature. Note that ERA5 and ERA5-Land share the same precipitation data, except for the higher spatial resolution of the latter.

230 Observed global land-surface precipitation and air temperature are taken from CRU TS (Climatic Research Unit gridded Time Series, v4.07). The dataset is derived by the interpolation of monthly climate anomalies from extensive networks of weather station observations (Harris et al., 2020) and is available at 0.5° x 0.5° spatial resolution and monthly temporal resolution, spanning the 1901–2022 period. The choice of this monthly product is driven by the fact that daily gridded observations for both temperature and precipitation were not readily available up to 2022 at the time of the analysis.

235 2.3 Land-surface characteristics and bioclimatic indicators

ESA CCI provides a set of ancillary datasets that were used in the generation of the products (Dorigo et al., 2021a). The ESA CCI soil porosity map has been used to convert ESA-CCI-ACT from the original units “percentage of saturation” to volumetric soil moisture in $\text{m}^3 \text{m}^{-3}$ as provided by the other considered products. The porosity map has been derived according to Saxton and Rawls (2006) taking clay, sand, silt, and organic matter of the Harmonized World Soil Database as

240 input.

For investigating impacts of land-surface and bioclimatic variables on the soil moisture trends in the various products (see Sect. 5.3), the latter are compared globally to those calculated using the maximum data availability over the 2000–2022 period for Vegetation Optical Depth (VOD; Zotta et al., 2024), ERA5-derived aridity (2000–2018 only; Wouters, 2021), and fractional covers of urban area, of bare soil and of tree cover (C3S, 2019).

3 Methods

3.1 Trend estimation

The analysis of trends is based on the yearly averages of the daily soil moisture data. For this, the daily soil moisture of the reanalysis products is masked for frozen soil conditions (based on the surface layer soil temperatures of the respective products), while ESA CCI soil moisture is already masked for this (Dorigo et al., 2017). Then, a mutual masking of all products is applied yielding in a consistent coverage. Trends are derived using the Theil-Sen trend estimator. Significance of the trends is determined with the Mann-Kendall test with a false rejection rate (or alpha value) of 0.05, and non-significant trends are masked for display of the trend maps when indicated. All trends are scaled to a denominator of $(20 \text{ yr})^{-1}$ to enhance readability and interpretability.

255

Apart from surface and root zone soil moisture, also trends in other relevant variables of the land water balance (i.e., total precipitation, evapotranspiration, runoff), as well as in surface air temperature are considered. For an easier comparison to these variables, we focus on trends in absolute soil moisture. These trends are based on yearly means of monthly data (see Sect. 2.2). In addition, we also look at trends in various land-surface characteristics and bioclimatic indicators (see Sect. 2.3).

260 3.2 Drought events characterisation

3.2.1 Event definitions

Based on guidance from the WMO (2016), extreme weather and climate events can be described quantitatively by a combination of the following metrics and information:

- An Index describing the anomaly from normal conditions (based on observations)
- 265 - A Threshold (above or below which conditions become 'extreme')
- Temporal information (records of the start date, end date, and duration)
- Spatial information (geographic area affected)

Here we focus on documented major drought events of the past two decades, with regions and periods that are predefined based on scientific literature and drought reports. From 2011 onward, in particular the Bulletin of the American

270

Meteorological Society (BAMS) “Explaining Extreme Events from a Climate Perspective” report series is considered for this purpose. These event definitions serve as spatial and temporal bounds for the characterisation of the individual drought events. An overview of the considered events and their predefined event regions and event periods is given in Supplementary Table 1. This analysis extends on the extreme event catalogue and event metrics developed within the C3S_511 (Crezee et al., 2019; Yang et al., 2022).

3.2.2 Index and drought metrics calculation

The soil moisture products considered here are given in volumetric moisture content (i.e., in units of $\text{m}^3 \text{m}^{-3}$), except for ESA-CCI-ACT which are originally in percent of saturation and converted to volumetric moisture content using the ESA CCI soil porosity map (see above). However, care needs to be taken when comparing absolute soil moisture from different sources since the absolute values are known to be dependent on underlying assumptions of the land-surface models and related soil property datasets (e.g., differing soil depths and soil properties like porosity) as well as on varying penetration depths of the remote-sensing products. We apply a standardization (Z -transformation) to remove differences in absolute levels and variability of the soil moisture values between the products, but also between locations, and focus on the temporal anomalies (see e.g., Koster et al., 2009; Orlowsky and Seneviratne, 2013).

285

These unitless standardised soil moisture anomalies (e.g., Orlowsky and Seneviratne, 2013) are based on daily input data and are calculated per individual grid point with respect to the climatology of the 2000–2022 reference period:

$$SMA_{y,d} = \frac{SM_{y,d} - \mu_d}{\sigma_d} \quad (1)$$

290

In Eq.1, $SM_{y,d}$ denotes soil moisture at any year y and day d , while μ_d and σ_d denote the climatological mean and inter-annual standard deviation of soil moisture of day d calculated over the reference period. To enhance the sample size, calculation of μ_d and σ_d for each day of the year is based on the days in a 11-day window around d , i.e., by applying a 11-day moving average on the original soil moisture time series. Note that a reference period identical to the analysis period is chosen in order to keep the calculation of the standardised anomalies independent of temporal fluctuations in the original time series prior to that, and to avoid reduced data coverage in the remote sensing products in earlier periods (e.g., Hirschi et al., 2023). A 3-day running mean is applied in addition on the resulting daily standardised anomalies with the purpose to fill daily gaps in the remote-sensing products.

295

For the definition of a drought, a threshold value of -1.5 standardised anomaly is chosen and any value below this is considered being in an abnormal dry state (i.e., $SMA_{y,d} < -1.5$). This threshold is inspired by the SPI-based categorization of droughts, where values below -1.5 represent severe to extreme drought (Mckee et al., 1993).

300

Four different metrics are defined for characterizing each drought event within the predefined event region and event period
305 (see Supplementary Table 1). The *magnitude* of the event is the minimum standardised anomaly over time. The *duration* of
the event is the total number of days (not necessarily consecutive) during the event for which the standardised anomaly is
below the threshold value of -1.5 . The *severity* is defined as the time-accumulated standardised anomalies over the days (i.e.,
consecutive, and non-consecutive) for which the standardised anomaly is below the threshold value. These metrics are all
calculated on the grid point scale. In addition, the temporally varying *spatial extent* of the event is defined as the area in
310 which the standardised anomaly is below the threshold of -1.5 .

Note that the application of the 3-day running mean smoothing of the standardised anomalies helps to fill temporal gaps in
the remote sensing products, while still being as close as possible to the original data. For the remote sensing products, a
larger smoothing window size (i.e., 5-day window) mainly impacts the calculation of the magnitude, while duration and
315 severity only slightly change. Also, sensitivity tests showed that there is not much impact of varying smoothing windows on
the results for the reanalysis products (not shown).

Since the severity captures both the duration and the amplitude of the event, it is suitable for defining the most affected *core*
of the event region as represented by the products. This core region is defined as all grid points for which the severity is
320 larger than the median of all non-zero severity grid points of the event and is used to spatially aggregate the drought metrics
for summarising the events.

4 Results

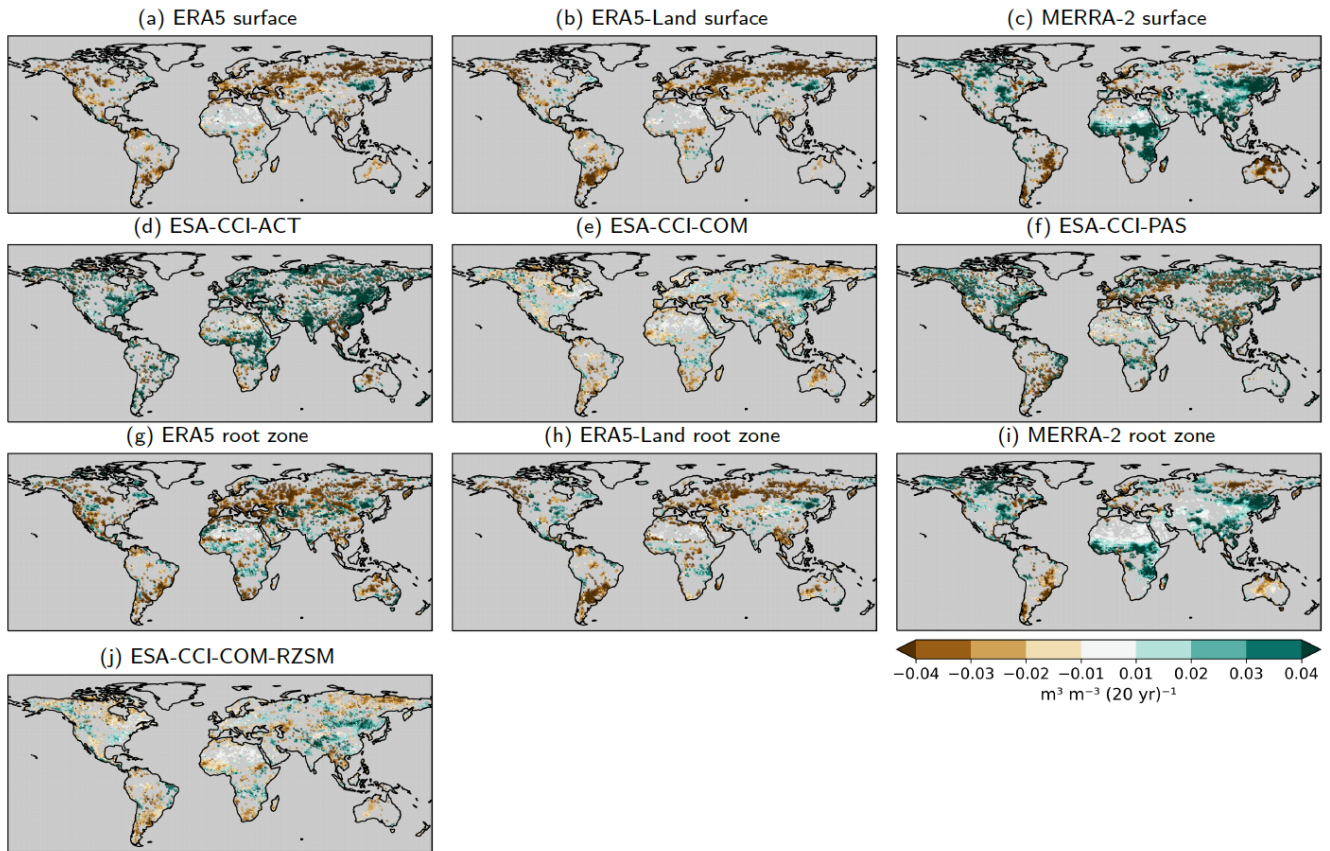
4.1 Trends in soil moisture

Among the remote-sensing products, ESA-CCI-COM and its root zone estimate ESA-CCI-COM-RZSM show more
325 widespread significant soil moisture drying trends, in particular in Siberia, the Black Sea/Caspian Sea region, southern
Africa, parts of South America and Australia (Fig. 1 d–f and j, cf. also Fig. 2). In contrast, ESA-CCI-ACT and to a lesser
extent -PAS display larger fractions and more pronounced wetting trends. Partly consistent drying trends in the ESA CCI
products (considering the trend direction, see Supplementary Fig. 1 a) can be observed in small parts of Siberia, in the
Caspian Sea region, parts of central Europe, southern South America and northern Australia, consistent wetting trends
330 mainly in Asia, North America, northwest Brazil and southeast Australia. Overall, the agreement in the trend direction is
limited among the ESA CCI products.

The reanalysis products ERA5 and ERA5-Land show mostly significant drying trends, particularly for surface soil moisture
(Fig. 1 a–b and g–h, Fig. 2). Strong and widespread drying can be observed in the northern mid- to high latitudes, in South

335 America, and central Africa, and in addition for the root zone also in southern Africa and parts of Australia. MERRA-2 in contrast displays widespread significant wetting trends in both surface and root zone soil moisture, except for South America, Australia, as well as parts of Siberia and Europe (Fig. 1 c and i). For the latter, consistent drying trends are observable in all reanalysis products (see also Supplementary Fig. 1 b). Consistent wetting trends in the reanalyses (Supplementary Fig. 1 b) can be observed in east Asia and India, parts of central Africa and North America, and in southeast

340 Australia, but these appear less widespread in ERA5/ERA5-Land compared to MERRA-2. Significant drying trends in ESA-CCI-COM, as well as ESA-CCI-COM-RZSM mostly agree with ERA5/ERA5-Land, wetting trends in Asia tend to agree more with MERRA-2.



345 **Figure 1** Theil-Sen trend estimate ($\text{m}^3 \text{m}^{-3} (20 \text{ yr})^{-1}$) on yearly mean soil moisture (based on daily data mutually masked for ESA CCI data availability and non-frozen soil conditions of the reanalysis products) in (a–f) the surface and (g–j) the root zone layer, 2000–2022 period. A Mann-Kendall test with a false rejection rate (or alpha value) of 0.05 was performed to mask out regions where no significant trend is present.

Of all products, ERA5-Land, ERA5 and ESA-CCI-COM, show largest area fractions of surface soil moisture drying trends (65.2, 65.2 and 59.1 % respectively, trends not masked for significance), while ESA-CCI-ACT and MERRA-2 show largest

350 fractions of wetting trends (63.8 and 59.0 % respectively; Fig. 2 a, Supplementary Table 2). Similarly, largest area fractions

of root zone soil moisture drying trends are present in ERA5, ERA5-Land and ESA-CCI-COM-RZSM (58.7, 57.8 and 58.3 %), and largest fractions of wetting trends in MERRA-2 (62.1 %). Nevertheless, some regions with largely consistent drying trends in all products (considering the trend direction, see also Supplementary Fig. 1 c) are apparent in parts of Europe, in the region northeast of the Caspian Sea, in southern Africa, northeast Australia and in parts of Siberia and South America.

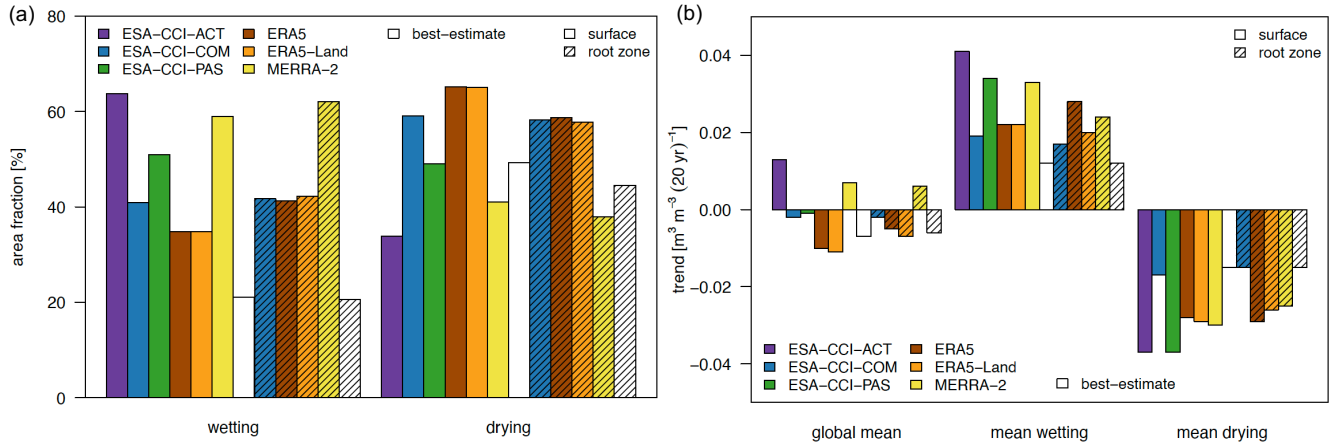


Figure 2 (a) Area fractions (in %) of wetting and drying trends within each product, as well as (b) their global mean trends and the respective mean wetting and drying trends (in $\text{m}^3 \text{m}^{-3} (20 \text{ yr})^{-1}$). Trends are not masked for significance, but for common spatial coverage of the datasets. The values for the best-estimate products (cf. Sect. 5.1) are based on the areas with trend direction consensus. Note that the respective numbers that are referred to in the text can be found in Supplementary Table 2.

Not only the area fractions of the trend directions diverge between the products, but also their trend magnitudes (Fig. 2 b). ESA-CCI-ACT and MERRA-2 show positive global means of the trends, while all other products show negative global means. The mean trend magnitudes in the wetting areas are largest for surface soil moisture of ESA-CCI-ACT and -PAS, as well as MERRA-2 ($0.03\text{--}0.04 \text{ m}^3 \text{m}^{-3} (20 \text{ yr})^{-1}$; Supplementary Table 2). Both ESA-CCI-ACT and -PAS also show largest drying trend magnitudes (around $-0.035 \text{ m}^3 \text{m}^{-3} (20 \text{ yr})^{-1}$). The mean drying is somewhat lower, but largely consistent between the reanalysis products (around $-0.03 \text{ m}^3 \text{m}^{-3} (20 \text{ yr})^{-1}$) for both surface and root zone soil moisture. The overall lowest trend magnitudes in both directions can be observed for ESA-CCI-COM and -RZSM (less than $0.02 \text{ m}^3 \text{m}^{-3} (20 \text{ yr})^{-1}$).

4.2 Drivers of soil moisture trends in the reanalysis products

To shed light on possible reasons for the observed differences in soil moisture trends between ERA5/ERA5-Land and MERRA-2, Fig. 3 displays the Theil-Sen trend estimates on yearly means of monthly precipitation, runoff, evapotranspiration and 2 m temperature (in addition to the trends in root zone soil moisture) for these products as well as for two gridded stations-based datasets of precipitation and temperature (both CRU). The patterns in precipitation trends (Fig. 3 a–b) of ERA5 and MERRA-2 show positive values in parts of east Asia and India, western USA, parts of east Africa, northern South America, and southeast Australia. Negative trends in both products are present in large parts of South

America and in northwest Australia. However, precipitation trends disagree in central Africa (trends negative in ERA5, but positive in MERRA-2), as well as southeast Asia (more widespread positive trends in MERRA-2). In addition, the positive trends in precipitation of MERRA-2 are often more pronounced and widespread compared to ERA5. While the pattern correlations with the observed precipitation trends (Fig. 3 c) are similar for ERA5 and MERRA-2 (0.33 for ERA5, respectively 0.34 for MERRA-2), precipitation trends of MERRA-2 display a positive mean bias ($0.171 \text{ mm d}^{-1} (20 \text{ yr})^{-1}$) and a larger RMSD ($0.847 \text{ mm d}^{-1} (20 \text{ yr})^{-1}$) compared to ERA5, which has a slight negative bias ($-0.004 \text{ mm d}^{-1} (20 \text{ yr})^{-1}$) and a lower RMSD ($0.492 \text{ mm d}^{-1} (20 \text{ yr})^{-1}$, see Supplementary Table 3). This results in larger differences between the reanalyses for trends in runoff and particularly for evapotranspiration (Fig. 3 d–i). In large parts of Asia, Africa and North America, trends in evapotranspiration are strongly and widespread positive in MERRA-2 while ERA5/ERA5-Land show more mixed or negative trends in these regions. These differences in evapotranspiration trends are reflected in the described differences in the soil moisture trends (Fig. 3 j–l, cf. Sect. 4.1). Supplementary Fig. 2 also shows the trends on yearly means of the cumulated monthly terrestrial water balance (i.e., precipitation minus evapotranspiration minus runoff, cumulated on annual basis). These trends in the annual terrestrial water balance (or terrestrial water storage) also show a relation to the trends seen in soil moisture, but also some differences. ERA5 and ERA5-Land particularly show more widespread wetting in terrestrial water storage than in soil moisture, while MERRA-2 shows more widespread drying. These differences are owed to components other than root zone soil moisture (i.e., deeper layer soil moisture and groundwater, snow, ice, biomass water) that contribute to terrestrial water storage and its trends.

The regional product differences in evapotranspiration and soil moisture trends also show a link to regional differences in 2 m temperature trends (Fig. 3 m–o). In the mentioned regions, the temperature trends for MERRA-2 are (more) negative, while ERA5/ERA5-Land show positive or only weak negative temperature trends. As for the precipitation trends, the temperature trends based on gridded observations (Fig. 3 p) in fact agree better with ERA5/ERA5-Land, while MERRA-2 overestimates the negative trends in Asia, Africa, and North America compared to the observations, resulting in a larger RMSD of $0.613 \text{ K} (20 \text{ yr})^{-1}$ of MERRA-2 compared to $0.536 \text{ K} (20 \text{ yr})^{-1}$ of ERA5 respectively $0.511 \text{ K} (20 \text{ yr})^{-1}$ of ERA5-Land (Supplementary Table 3). Corresponding pattern correlations with the observed temperature trends amount to 0.65 for MERRA-2 and ERA5, and to 0.7 for ERA5-Land, with a negative mean bias of $-0.219 \text{ K} (20 \text{ yr})^{-1}$ for MERRA-2 compared to a positive bias for ERA5 (ERA5-Land) of $0.221 \text{ K} (20 \text{ yr})^{-1}$ ($0.238 \text{ K} (20 \text{ yr})^{-1}$).

Overall, the lower biases in precipitation trends of ERA5 and the stronger constraint with observed regional temperature trends results in more widespread soil drying and evapotranspiration decreases of both ERA5 and ERA5-Land. In contrast, in MERRA-2 the overly positive trends in precipitation translate into enhanced soil moisture and evapotranspiration and a resulting stronger regional cooling, which is less in line with the observed temperature trends.

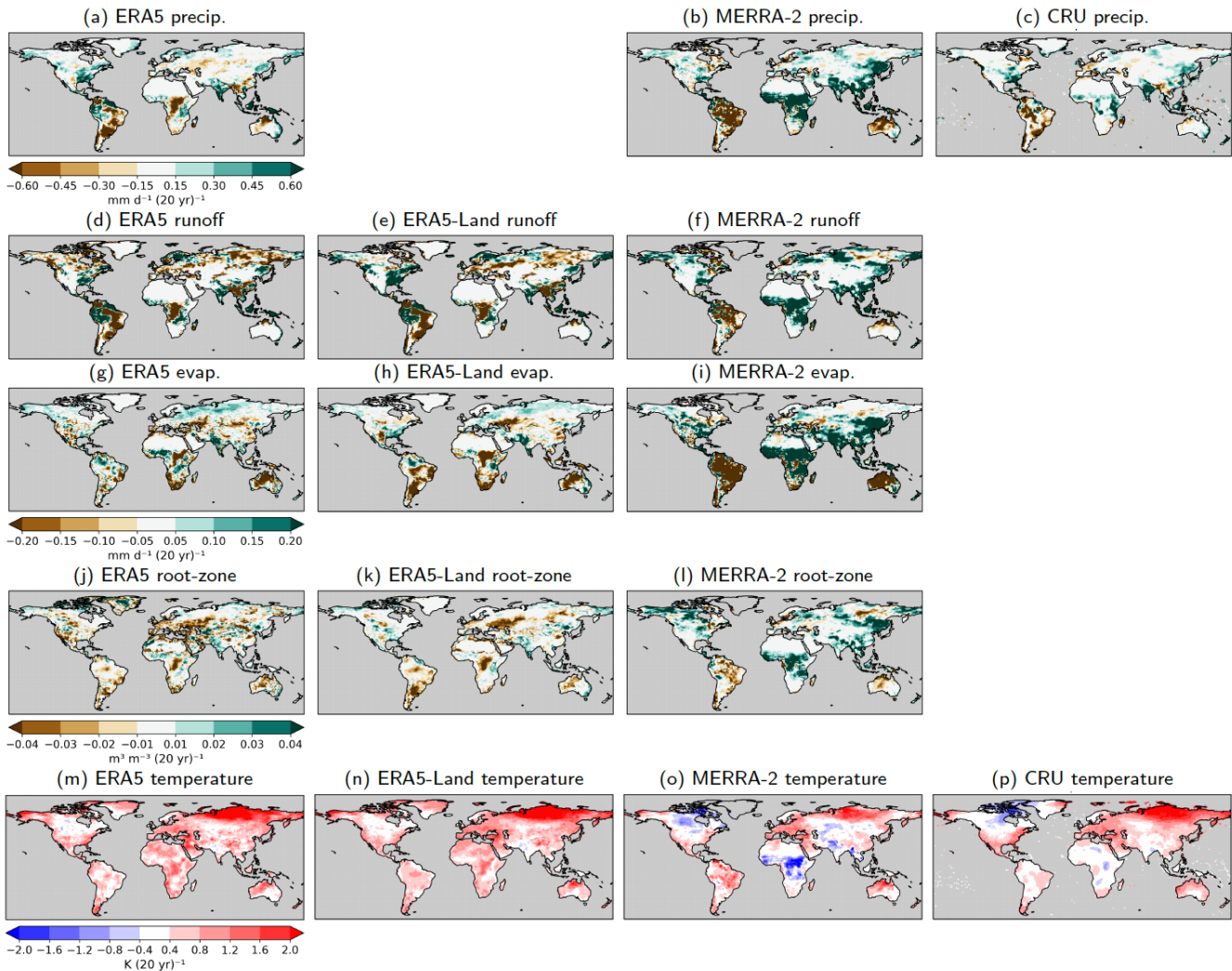


Figure 3 Theil-Sen trend estimate (2000–2022 period) on yearly means of monthly precipitation (a–c), runoff (d–f), evapotranspiration (g–i), root zone soil moisture (j–l) and surface air temperature (m–p) from the reanalysis products as well as two gridded stations-based datasets for precipitation and temperature. Values are in $\text{mm d}^{-1} (20 \text{ yr})^{-1}$ for the fluxes, respectively $\text{m}^3 \text{m}^{-3} (20 \text{ yr})^{-1}$ for soil moisture and $\text{K} (20 \text{ yr})^{-1}$ for temperature. Regions with non-significant trends are not masked out for easier comparison with the trends in soil moisture. Note that ERA5-Land is forced by ERA5 precipitation and is thus not shown for the former.

415

4.3 2022 Drought in Europe

In the following, we investigate the products' ability to capture major agroecological drought events as a use case. Detailed results are presented for the 2022 drought in Western-Central Europe (Schumacher et al., 2022; Schumacher et al., 2024) as an example. This is followed by the characterization of multiple recent major drought events worldwide considering all products (Sect. 4.4) and the product intercomparison based on these events (Sect. 4.5).

420

The severity of the 2022 drought event appears largest in central and western Europe, with highest values based on surface soil moisture in Germany, Switzerland, France, Italy as well as parts of eastern Europe (Fig. 4 a–f). This core of the event region (see Sect. 3.2.2) is captured by all products, but the region appears less coherent in the ESA-CCI-ACT (and partly -PAS) remote sensing product. Due to the strong correlation of surface soil moisture with deeper soil layers (e.g., Hirschi et al., 2014), the location of the event in the root zone is very similar compared to the surface layer (Fig. 4 g–j). However, the core region is less coherent and widespread in the root zone (cf. also horizontal line segments of Fig. 7 b, which indicate the spatial extent of the core region).

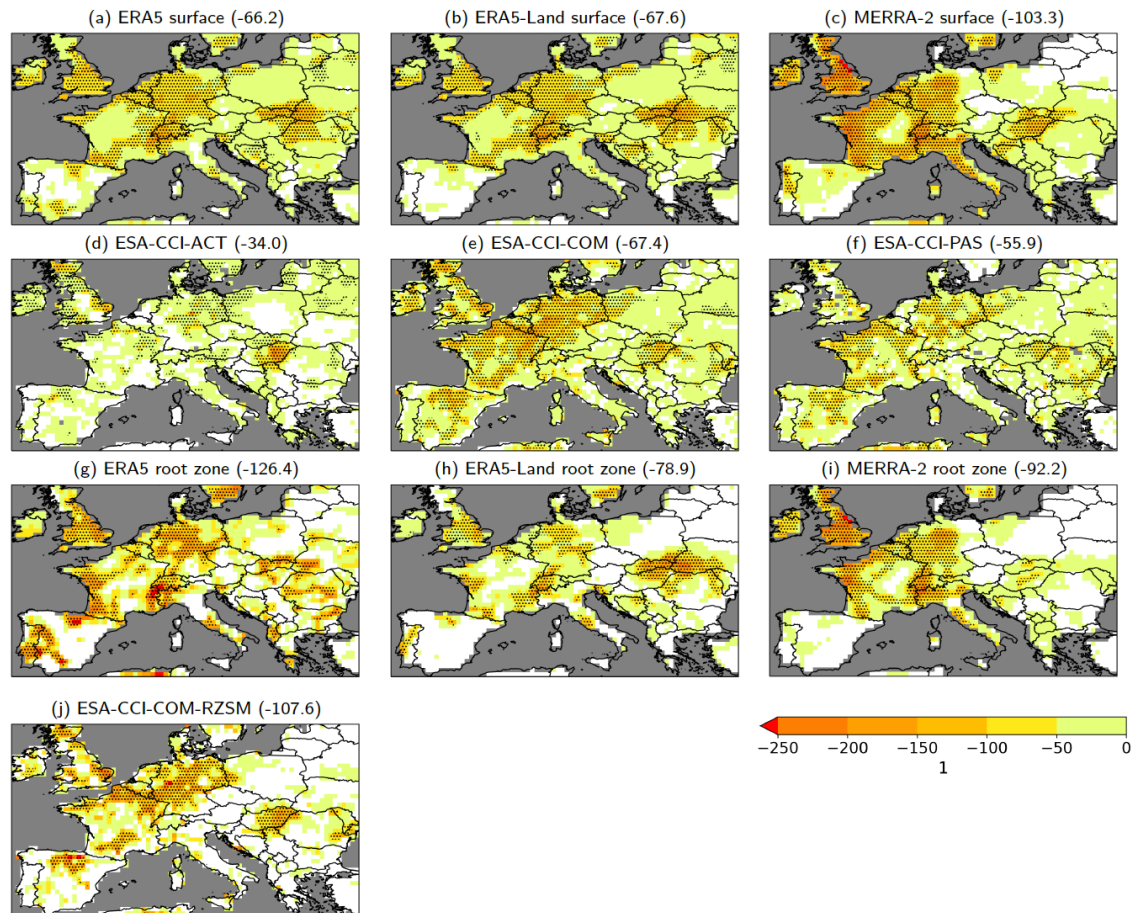
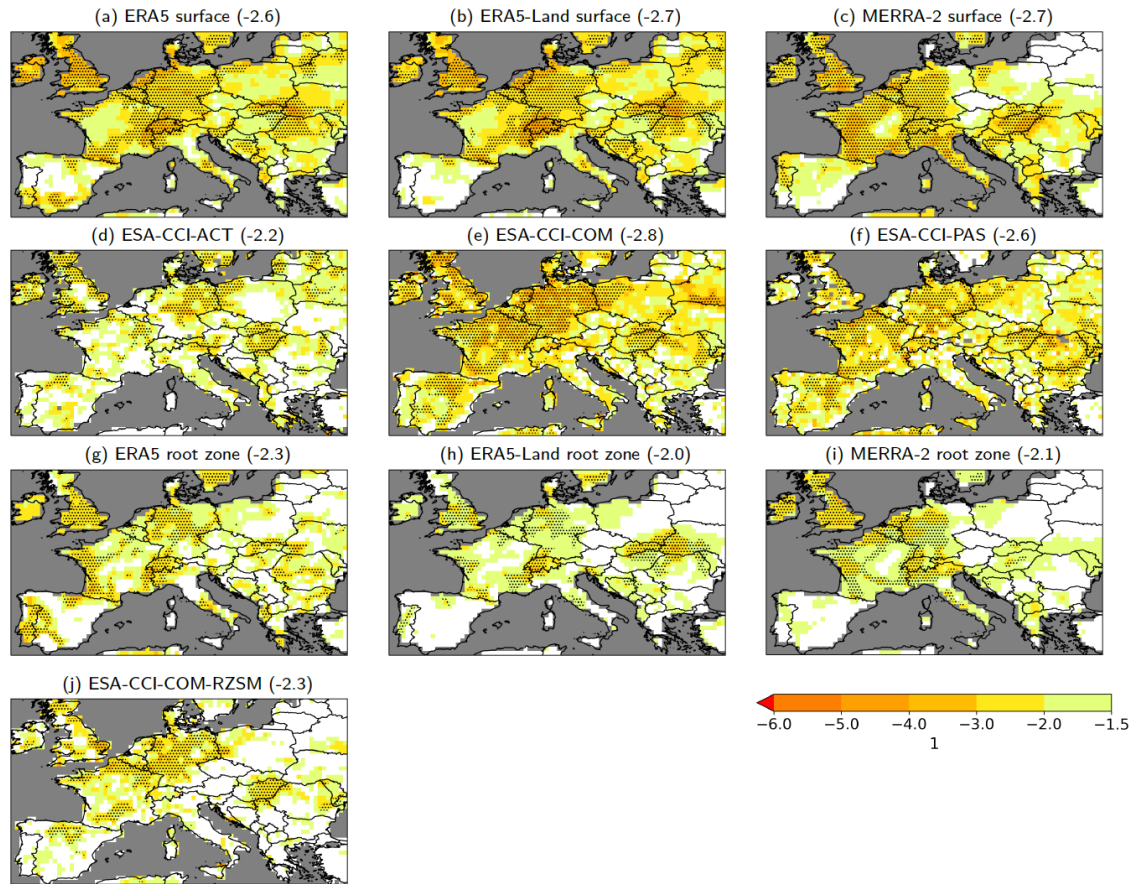


Figure 4 Severity of the Europe 2022 drought event (in units of standard deviations) based on the time-accumulated soil moisture anomalies in (a–f) the surface and (g–j) the root zone layer. The core of the event region is stippled, and the area mean of the severity over the respective core of the event region is denoted in brackets.

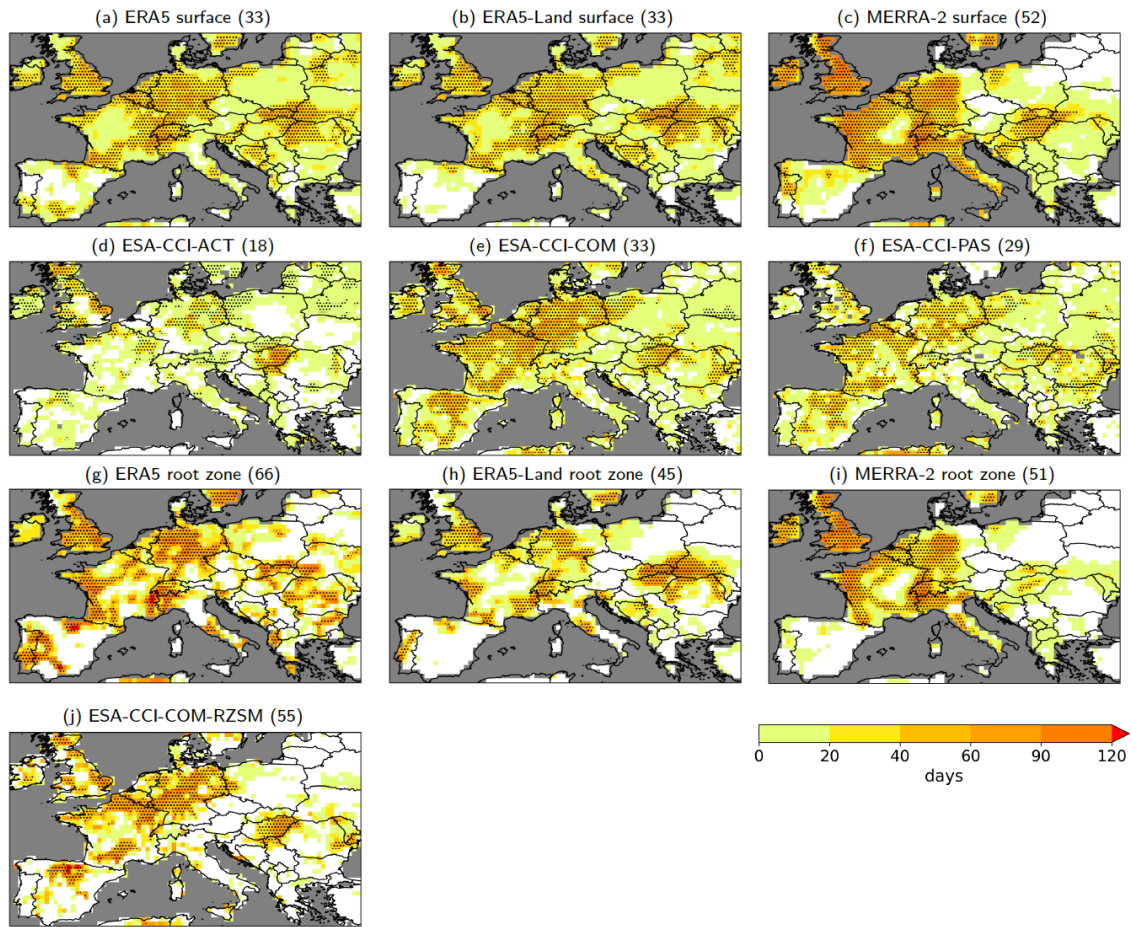
For surface layer soil moisture, the event appears most severe in MERRA-2 (though within a smaller extent of the core region than the other reanalyses), followed by ERA5-Land, ESA-CCI-COM, and ERA5 (Fig. 4, see also Supplementary

Table 4 for an overview of all drought metrics of the Europe 2022 event). ESA-CCI-ACT shows weaker severities for this event. The magnitude of the 2022 European drought based on ESA-CCI-COM and -PAS is over large parts comparable to the reanalysis products, with standardised anomalies of -3 and less in parts of the core region of the event (Fig. 5). ESA-CCI-ACT shows weaker magnitudes. The event shows the longest durations in MERRA-2, with over 90 days in parts of the core region and over 50 days on the average over it (Fig. 6). ERA5/ERA5-Land and ESA-CCI-COM and -PAS display average durations of around 30 days, and ESA-CCI-ACT the shortest with 18 days.



445

Figure 5 Magnitude of the Europe 2022 drought event (in units of standard deviations) based on the temporal minimum of the standardised soil moisture anomalies in (a–f) the surface and (g–j) the root zone layer. The core of the event region is stippled, and the area mean of the magnitude over the respective core of the event region is denoted in brackets.



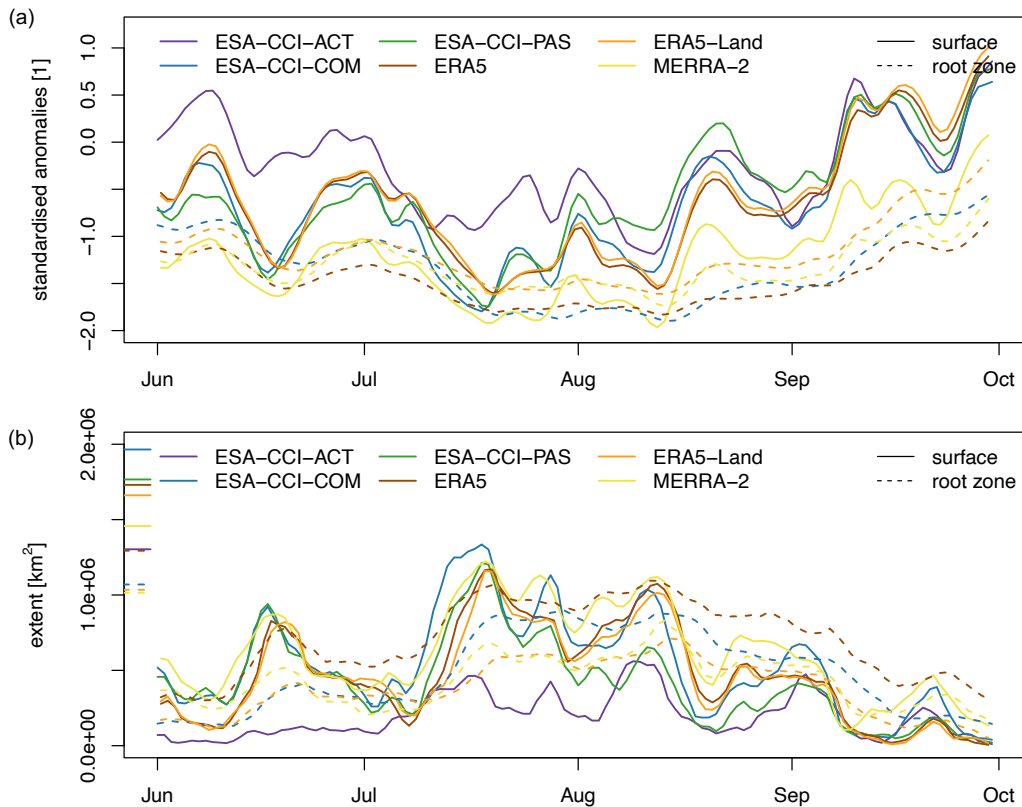
450 **Figure 6 Duration of the Europe 2022 drought event (in days) based on the number of days within the event period with standardised soil moisture anomalies below -1.5 in (a–f) the surface and (g–j) the root zone layer. The core of the event region is stippled, and the area mean of the duration over the respective core of the event region is denoted in brackets.**

In the root zone of ERA5-Land and particularly of ERA5 and ESA-CCI-COM-RZSM, the 2022 European drought appears more severe as compared to the surface layer (Fig. 4, see also Supplementary Table 4) mostly due to longer durations
 455 (Fig. 6), while the magnitudes are weaker (Fig. 5). MERRA-2 shows a similarly reduced drought magnitude in the root zone as ERA5/ERA5-Land, but in contrast, the duration is similar as in the surface layer (where it is however already substantially longer than in ERA5/ERA5-Land). Together with partly weaker negative anomalies (cf. Fig. 7 a), the severity in the root zone of MERRA-2 as a result becomes reduced compared to the surface layer.

460 The temporal evolution of the standardised surface soil moisture anomalies averaged over the core of the event region shows two strongest phases of the event in the second half of July and first half of August 2022 (Fig. 7 a), with average standardised anomalies based on the reanalysis products reaching -1.5 . Anomalies are most pronounced (i.e., close to -2) and prolonged for MERRA-2 compared to the other products. ERA5 and ERA5-Land show weaker negative anomalies and a

quicker return to normal conditions. Among the remote-sensing products, ESA-CCI-COM and -PAS show the most negative anomalies, however with the minimum in the second half of July. Over the whole period, ESA-CCI-ACT show overall weakest standardised anomalies, which are on average only shortly below normal conditions.

Root zone soil moisture anomalies from the reanalysis products display less temporal variation, with longer-lasting minimum values in July and August (dashed lines in Fig. 7 a). In the root zone, the dryer than normal conditions persist during late summer and early autumn, with values still below -1 standardised anomaly. Strongest and most prolonged root zone soil moisture anomalies are displayed by ERA5 and ESA-CCI-COM-RZSM, while ERA5-Land and MERRA-2 show weaker negative anomalies.



475 **Figure 7 (a) Average of the standardised surface (full lines) and root zone (dashed lines) soil moisture anomalies within the**
respective core of the event regions (cf. stippled regions in Figs. 4–6) during the Europe 2022 drought event period. (b) Spatial
extent of the standardised surface (full lines) and root zone (dashed lines) soil moisture anomalies below -1.5 within the core of the
event region during the Europe 2022 drought event (full lines). Line segments at the left border of the figure indicate the extent of
the core region for each dataset (i.e., corresponding to the extents of the stippled areas of Figs. 4–6 where the severity is larger than
the median of all non-zero severity grid points).

The temporal evolution of the spatial extent of the drought (i.e., the area of standardised soil moisture anomalies below -1.5 within the core of the event region) shows highest values during July, reaching over 1.3 Mio. km² for surface soil moisture of

485 ESA-CCI-COM (Fig. 7 b, Supplementary Table 4) followed by 1.2 Mio. km² of MERRA-2 and ESA-CCI-PAS. The maximum spatial extent of the event in the root zone is clearly lower compared to the respective surface layer in ERA5-Land, MERRA-2 and ESA-CCI-COM-RZSM, while it is less reduced in ERA5. Correspondingly, ERA5 shows the largest spatial extent of the drought in the root zone with a maximum of 1.09 Mio. km², followed by ESA-CCI-COM-RZSM with 0.90 Mio. km² (Supplementary Table 4).

4.4 Recent major drought events

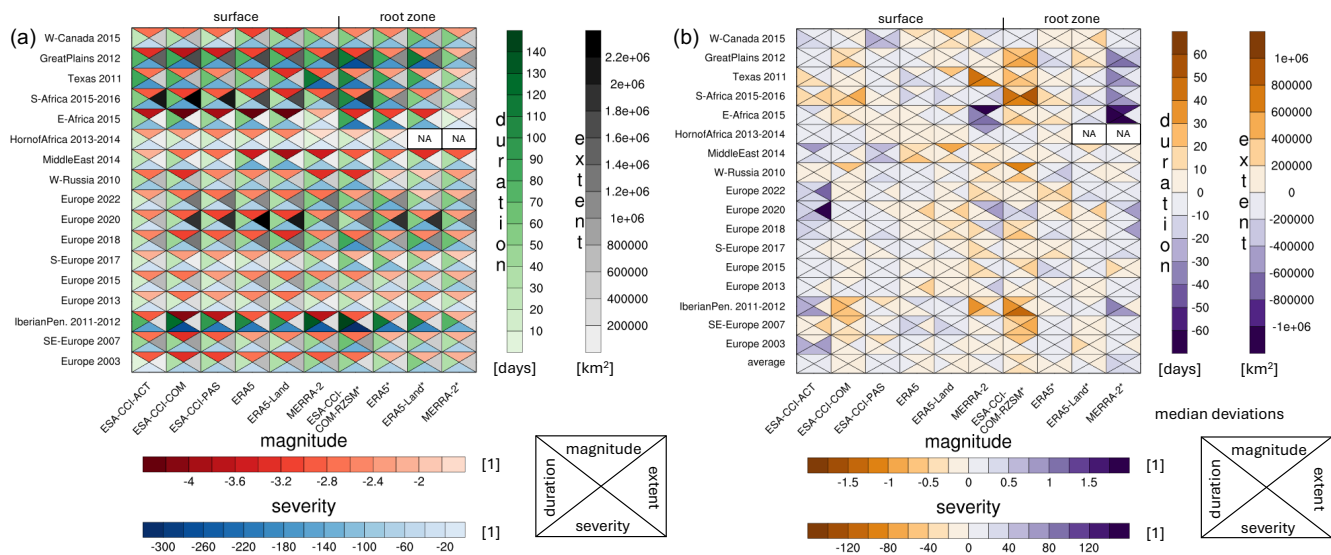
490 An overview of the characteristics of major drought events in the 2000–2022 period as represented in the various products is given in Fig. 8 a (based on surface and root zone soil moisture).

The Iberian Peninsula 2011–2012 drought and the Texas 2011 and Great Plains 2012 droughts appear most severe and longest in most of the products and both surface and root zone layer. The East Africa drought of 2015 shows overall strongest magnitudes (except in MERRA-2), followed by Iberian Peninsula 2011–2012 drought. The spatial extents of the drought reach highest values for the Europe 2020 and the South Africa 2015–2016 droughts, though with large differences between the products. In the root zone, the drought events appear weaker in terms of magnitudes, often prolonged and partly more severe.

500 As for the 2022 drought event in Europe, ESA-CCI-ACT often displays weaker droughts in all metrics compared to the ESA-CCI-COM and the ERA5/ERA5-Land products. This is also visible in Fig. 8 b, which displays the respective product deviations in the drought metrics with respect to the product median of each event as a baseline. The weaker drought representation of ESA-CCI-ACT is particularly pronounced for events in Europe and is evident in all metrics (on average over all events +17 in severity, +0.2 in magnitude, –6 days in duration, and –129'000 km² in spatial extent). Also MERRA-2 shows weaker droughts in the root zone compared to the other products, which is most evident for events in North America and Africa (+33 in severity, +0.25 in magnitude, –14 days in duration, and –105'000 km² in spatial extent on average over all events). In the surface layer, the deviations of MERRA-2 are more mixed, with a weaker representation of the East Africa 2015 drought, but a stronger representation (particularly in terms of duration and severity) of the Texas 2011 and Iberian Peninsula 2011–2012 droughts. For other events, durations also tend to be prolonged and corresponding severities increased in MERRA-2 surface soil moisture, while the magnitudes are partly weaker and spatial extents smaller.

510

Compared to the reanalysis products, ESA-CCI-COM-RZSM shows partly stronger drought severities and corresponding longer event durations (e.g., Iberian Peninsula 2011–2012, South Africa 2015–2016, Texas 2011), as well as often stronger magnitudes. Also, the spatial extents of the droughts appear larger in some cases in ESA-CCI-COM-RZSM (e.g., Southeast Europe 2007, South Africa 2015–2016, Great Plains 2012).



515

Figure 8 (a) Drought metrics of recent major drought events. The values are based on surface soil moisture and root zone soil moisture (products denoted with *) and represent the area mean over the respective core of the event region in case of severity, magnitude, and duration, and the temporal maximum in case of the spatial extent. (b) Product deviations in these drought metrics with respect to the product median of each event, separately calculated for the surface and the root zone (i.e., comparable to the product deviations that are shown in Fig. 11 and Supplementary Figs. 3 and 4). In this case, also the average of the product median deviations is shown for the individual products. NA is displayed when products do not exhibit standardized anomalies below -1.5 for a specific event.

520

4.5 Product intercomparison

The overall product behaviour during the analysed drought events is summarised in Fig. 9. In line with the results of the previous sections, the dampened drought magnitudes and smaller spatial extents in the root zone compared to the surface layer are again visible in the respective products. Also, a tendency to prolonged durations and stronger severities of the droughts in the root zone is observable (except for MERRA-2, which already shows partly longer durations in the surface layer compared to the other products). ESA-CCI-COM-RZSM displays partly stronger representation of the drought severities and particularly magnitudes compared to the reanalysis products, while MERRA-2 shows weaker drought magnitudes and partly shorter durations and lower severities.

530

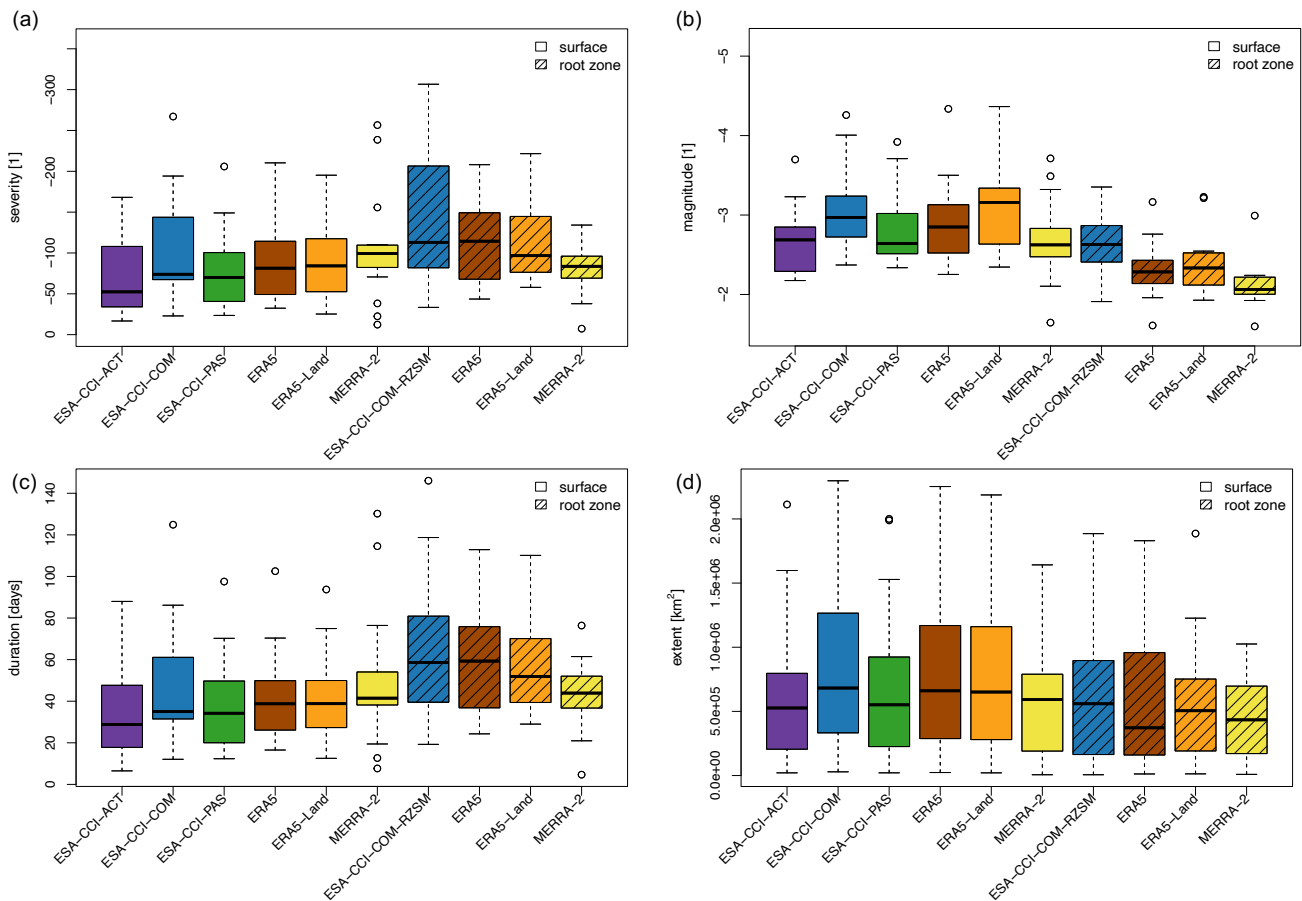


Figure 9 Product intercomparison based on the drought metrics (a) severity, (b) magnitude, (c) duration, and (d) spatial extent. The box-whisker plots represent the distributions of the drought metrics for the analysed 17 drought events.

535 For surface soil moisture, the ESA-CCI-ACT, and to a lesser extent the ESA-CCI-PAS products, tend to show partly weaker drought signals in all presented metrics compared to ESA-CCI-COM and ERA5/ERA5-Land. This is most pronounced for the drought magnitudes of ESA-CCI-ACT. Similar as for the root zone, ESA-CCI-COM displays partly stronger drought severities (cf. ESA-CCI-COM-RZSM) and longer durations. As for the root zone, MERRA-2 displays weaker drought magnitudes compared to the other products, while particularly shorter droughts appear partly prolonged (and more severe) in
 540 its surface layer (cf. also the Europe 2022 drought above and corresponding Figs. 4–6, and Supplementary Table 4, as well as Fig. 8 for all events).

The spatial extents of the droughts based on surface soil moisture tend to be larger for ESA-CCI-COM and ERA5/ERA-Land, particularly for larger droughts. In the root zone, the spatial extents of larger droughts tend to be smaller.

545

Appendix A furthermore provides an intercomparison of the products based on their spatial drought metrics patterns. Fig. A1 shows the pairwise pattern correlations and RMSDs of severity, magnitude and duration (cf. Figs. 4–6 for the Europe 2022 drought) as represented by the products. The Pearson correlations between the patterns of the products are overall positive and significant for all metrics, showing the general product agreement of the location and spatial variation of the considered droughts. The correlations between products are similar for severity and duration (which are related by design, see Sect. 3.2.2) but tend to be lower for the drought magnitude. As expected, related products (i.e., ERA5/ERA5-Land, ESA-CCI-COM/-RZSM), as well as surface and corresponding root zone soil moisture products show closest agreement with correlations ≥ 0.6 for severity and duration (and ≥ 0.5 for magnitude). Similarly, correlations between the satellite products also amount to ≥ 0.6 for severity and duration but tend to be lower for magnitude. The patterns of the RMSD values are less distinct, but ERA5/ERA5-Land and ESA-CCI-COM show comparably lower values for severity and duration, while ESA-CCI-COM-RZSM and MERRA-2 tend to show largest values.

5 Discussion

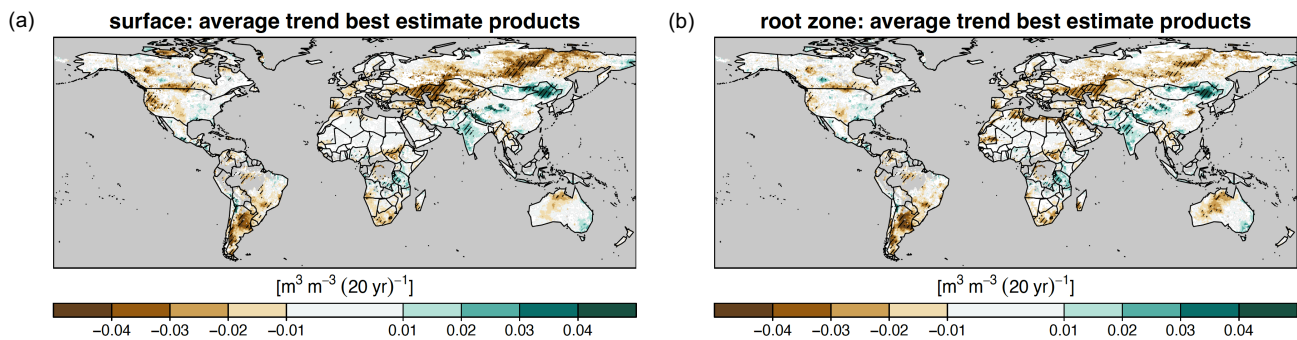
5.1 Synthesis of soil moisture trends

Section 4.2 has shown that ERA5/ERA5-Land appear more consistent with observed precipitation and temperature trends. The resulting more widespread soil drying and evapotranspiration decreases can thus be assumed to be more realistic in these products than in MERRA-2. In contrast to ERA5, MERRA-2 does not benefit from an analysis of synoptic surface air temperature observations (Simmons et al., 2017), and is thus less constrained by ground observations. This could explain the identified regional negative biases in 2 m temperature trends of MERRA-2 compared to ERA5. The latter includes an assimilation of these ground-based surface air temperature measurements, from which also ERA5-Land indirectly benefits. In addition, the assimilation of 2 m temperature and relative humidity pseudo-observations in the soil moisture analysis of ERA5 tend to have an important impact on root zone soil moisture and latent/sensible heat fluxes (Fairbairn et al., 2019), which could contribute to the higher sensitivity of ERA5 to drought events.

Apart from the impact of differences in the forcing and in the data assimilation strategies on the observed soil moisture trends of the reanalyses, differing land-surface model parametrisations may further contribute to product-specific drought representation and trends of the reanalyses. In particular, MERRA-2 has been shown to exhibit a prolonged surface soil moisture memory (Dirmeyer et al., 2016; cf. Fig. 6 therein), which contributes to the observed partly prolonged durations (and stronger severities) of shorter droughts in the surface layer of this product. Also, He et al. (2023) report that in water-limited evapotranspiration regimes, MERRA-2 shows a larger overestimation of soil moisture memory times compared to estimates from SMAP, while the bias in ERA5 is lower. It is noted that soil moisture thresholds (i.e., wilting point and critical point; see e.g., Seneviratne et al., 2010) in the land-surface model parametrisations contribute to the observed differences in the soil moisture memory times. Comparing these soil moisture thresholds between ERA5 (based on

HTESSEL) and MERRA-2 (based on the CLSM) reveals that both the wilting point and particularly the critical point tend to be higher for ERA5 than for MERRA-2 (cf. also Schwingshackl et al., 2017, Fig. 14 therein). This may translate into the observed stronger drought representation of ERA5 since it more quickly enters a soil moisture limited evapotranspiration regime during dry downs.

Previously, ERA5/ERA5-Land and MERRA-2 soil moisture were jointly evaluated with other reanalyses against in situ observations from various networks (Li et al., 2020; Beck et al., 2021; Zheng et al., 2024). On the network scale, ERA5 showed higher consistency with observed soil moisture compared to MERRA-2 based on temporal correlation coefficients and standard deviations, as well as when considering the correlations of the seasonal trend decomposed time series (Li et al., 2020). Furthermore, ERA5-Land soil moisture shows a consistent improvement compared to ERA5 based on a large set of in situ observations (Beck et al., 2021; Muñoz-Sabater et al., 2021). The improvement is more marked for root zone soil moisture than for surface soil moisture. Also, compared to Cosmic Ray Neutron Sensor observations, ERA5-Land outperforms MERRA-2 (Zheng et al., 2024). Within the remote-sensing products, available validation studies indicate that ESA-CCI-COM outperforms the individual ESA-CCI-ACT and ESA-CCI-PAS products when compared to in situ soil moisture measurements (Gruber et al., 2019; Beck et al., 2021; Hirschi et al., 2023). Also, previous studies point to artificial wetting trends in ASCAT soil moisture in areas of widespread deforestation or urban growth (Hahn et al., 2023). This is reflected in the observed larger fractions of wetting trends of ESA-CCI-ACT, which since 2007 is solely based on ASCAT observations. Given these available evaluation studies and the identified biases in MERRA-2 precipitation and temperature trends (Sect. 4.2), in the following we only consider the ESA-CCI-COM-based products and ERA5-Land for a synthesis on the global surface and root zone soil moisture trends based on these best-estimate products. It should be noted that ESA-CCI-COM-RZSM is unlikely to show surface to root zone de-coupling in trends given the exponential filter derivation.



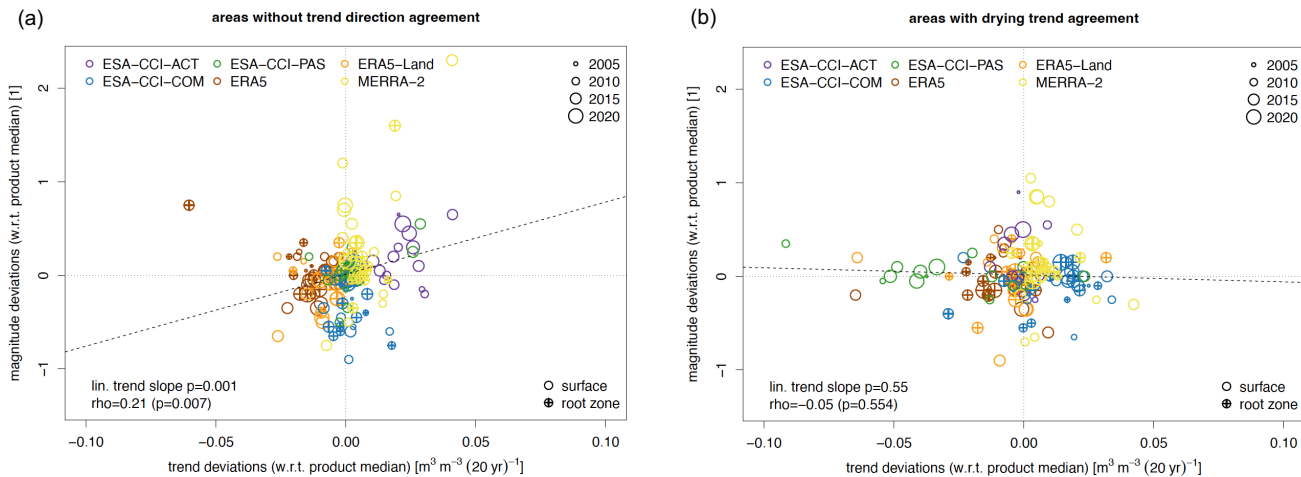
600 **Figure 10** Best-estimate products average of 2000–2022 Theil-Sen trends ($m^3 m^{-3} (20 yr)^{-1}$) on yearly mean (a) surface and (b) root zone soil moisture. Underlying daily data is masked based on the ESA-CCI-COM (a) (and -RZSM, b) data availability, and non-frozen soil conditions of ERA5-Land (a, b). The mean trends are only shown in areas with trend direction agreement of both respective best-estimate products, while white colour denotes no consensus in the trend direction. Additionally, areas of common significant trends are hatched.

605 Based on the average of the respective two best-estimate products' trends (Fig. 10), common soil moisture drying can be observed in Siberia, in the region of the Black Sea/Caspian Sea and Central Asia, in parts of Europe and the Mediterranean, parts of western USA and the Canadian Prairies, as well as larger parts of South America, parts of southern and northern Africa and northwest Australia. These drying trends are often significant in both products ($p < 0.05$; cf. hatched areas in Fig. 10), and the regions are mostly consistent with previous studies on trends in water availability (e.g., Padron et al., 2020).
610 Common wetting trends are present in East Asia and India, southeast Australia, and in eastern Africa. Common significant wetting trends appear less widespread than drying trends and are mostly refined to parts of Asia and central and eastern Africa.

The corresponding global area fractions of common soil moisture drying trends amount to 49.3% for the surface soil layer, and to about 44.5% for the root zone (Fig. 2 a, Supplementary Table 2). The respective wetting trends amount to 21.1% (surface) respectively 20.6% (root zone), and areas with no trend direction consensus to 29.6% respectively 35.0%, reflecting the considerable uncertainties associated with global soil moisture trends.

5.2 Relation of drought representation and soil moisture trends

In the following, we investigate the effect of the diverse and partly contradictory soil moisture trends of the products on their representation of the investigated drought events. For each event and product, Fig. 11 shows the product deviation in the representation of these events in terms of magnitude versus the deviation in the 2000–2022 trend. The analysis is stratified by separating the drought regions in areas with drying trend agreement and in those without trend direction agreement (cf. Supplementary Fig. 1 c, brown respectively white areas). Trends and magnitudes are averaged over these respective areas, and the respective deviations are calculated with respect to the product median of each event. The chronology of the events
625 within the 2000–2022 period is indicated with increasing circle sizes.



630 **Figure 11 Product deviations in drought magnitude as a function of product deviations in the 2000–2022 soil moisture trends, with circle sizes depending on the chronology of the events within the investigated period (i.e., later events are displayed with larger circles). (a) Relation in areas without trend direction agreement of the products, (b) relation in areas with drying trend agreement. Deviations are displayed with respect to the product median of each event, separately calculated for the surface and the root zone (the latter additionally indicated with a “+”). The trends and drought magnitudes are averaged over the respective areas of drying trend agreement and trend direction disagreement within the drought regions. The p-values of the linear trend slope (dashed line) and the Spearman rank correlation rho between the drought metrics and the soil moisture trends are noted as well.**

635 The scatter plots reveal that in areas without trend direction agreement (Fig. 11 a), a significant relation between deviations in drought magnitude and deviations in the trend is present. Thus, as expected, products with negative (positive) deviations in the trends are connected with stronger (respectively weaker) drought magnitudes (i.e., corresponding to negative respectively positive deviations in the magnitude). The scatter plot of Fig. 11 a also indicates a temporal dependency of the deviations, as the largest deviations tend to relate to events occurring after around 2010, which further shows the importance of the trend representation on the products' ability to detect droughts. However, in areas with drying trend agreement of the products (Fig. 11 b), such a relation between product deviations in the drought magnitude and the corresponding deviations in the trend is not present. Analogous results are obtained by considering the severity of drought events rather than their magnitude (Supplementary Fig. 3). Thus, consensus in the soil moisture drying results in more consistent drought signals of the products. Overall, this analysis highlights that the trend representation has a significant influence on the drought-detection capacity of the products.

650 For the ESA-CCI-ACT and MERRA-2, the positive deviations in the trends and the reduced drought magnitudes and severities are visible in the location of several events in the respective upper right quadrant (Fig. 11 a, Supplementary Fig. 3 a). These are the products that show larger area fractions of positive than negative trends (cf. Fig. 2 a, Supplementary Table 2). ESA-CCI-ACT also exhibits an intensification and extension of the wetting trends in the later part of the analysis period (compared to the 2000–2022 period, not shown), which further contributes to the reduced drought magnitudes of later

events. An additional contribution may come from sensing issues of active microwave remote sensing during dry spells, which lead to an increase in the backscatter of the signal due to subsurface scattering, resulting in an erroneous increase in soil moisture (Wagner et al., 2022).

655

Apart from the trend representation, also the inter-annual variability of soil moisture may contribute to the drought-detection capacity of the products. This is investigated by relating the product deviations in drought severity and magnitude to the product deviations in the inter-annual variability of the standardised soil moisture anomalies. The inter-annual variability is characterised by the standard deviation of the annual mean standardised soil moisture anomalies of the 2000–2022 period, which are detrended using a LOWESS filter. Supplementary Fig. 4 a indicates a significant relation between drought severity and the inter-annual variability of soil moisture. Thus, products with larger inter-annual variability in soil moisture display stronger drought severities. However, such a relation is not evident for the drought magnitudes, which show no significant relation with inter-annual soil moisture variability (Supplementary Fig. 4 b). This may be because magnitude represents only one day of each event (i.e., the temporal minimum of the standardised anomalies during the drought period), whereas severity is calculated as the accumulated standardised anomalies over all days below the drought threshold and thus tends to be more related to the annual mean of the anomalies.

660

665

5.3 Impact of land-surface/bioclimate variables on satellite soil moisture retrieval and modelling uncertainties

The detected differences in trend (and consequent drought) representation of reanalysis and remote-sensing products (Fig. 1) have partly been reported previously (e.g., Dorigo et al., 2012; Preimesberger et al., 2021). Past studies have linked them to fundamental modelling simplifications in the description of human impacts, which may explain differences regionally (Qiu et al., 2016). However, differences result also from the intrinsic trend representation error of the satellite products. The evidence of locally contradicting trends between the considered ESA-CCI-ACT, -PAS, and -COM (Fig. 1) suggests that the differences in the observation system and retrieval algorithm used in the various products have a non-negligible effect on their trend- and drought-detection capacity.

675

The presented trend analysis is bound to deal with the heterogeneities in the true spatial support and sampling frequency of the products, which can explain part of the observed deviations if accounted for explicitly (Wen et al., 2022). In this respect, the satellite products are set apart by the lower observational density that results from ingesting (in the 2000–2022 analysis period) four sensors in the ACTIVE products against more than double that amount in PASSIVE and COMBINED. This affects the noise levels and – remarkably – their rate of change over time (Hirschi et al., 2023), which leads to biased trends. On top of this, the individual sensors are subject to their own performance drift (Fennig et al., 2020), that propagates to the merged products but is virtually impossible to isolate in the merged soil moisture signal. Generally, spurious trends are also attributed to non-resolved inter-sensor biases in the merging process (Yang et al., 2013). However, this was not found to be the case in antecedent product versions of the considered ESA CCI products (Preimesberger et al., 2021; Su et al., 2016).

680

Dynamic processes on the land-surface present an additional potential impediment to the stability of the soil moisture retrieval and the reanalysis-based soil moisture (and thus trends and anomalies representation). Retrieval algorithms as well as the land-surface models underlying the reanalyses may in fact be grounded on stationarity assumptions that are challenged by evolving land-surface characteristics. For instance, the vegetation correction of the H SAF ASCAT soil moisture record ingested in the ESA-CCI-ACT and -COM products is parametrised on a seasonal basis in the TU Wien model (Naeimi et al., 2009; H SAF, 2021), thus not accounting for inter-annual differences and trends in vegetation (Vreugdenhil et al., 2016). This may introduce biases over time, leading to an inconsistent representation of the anomalies and to spurious trends in certain areas. The same effect would be caused by temporal variations of the statically calibrated dry- and wet-reference, following soil porosity variations. Abrupt land cover changes are also not automatically parametrised and cause artificial trends which should be visible for instance in areas of widespread deforestation or urban growth (Hahn et al., 2023).

Based on the above, trends in the remote sensing and the reanalysis products – or at least differences between them – might be explained by considering the underlying trends of relevant land-surface characteristics and bioclimatic indicators. Hence, trends in soil moisture are compared globally to those calculated using the maximum data availability over the 2000–2022 period for VOD, ERA5-derived aridity (2000–2018 only), and fractional covers of urban area, of bare soil and of tree cover, and the results are included in Appendix A. The VOD data is masked consistently as for the soil moisture trends; this was not possible for the other variables as they were already aggregated above the daily level in the original products. In case of aridity, there appears to be a strong explanatory capacity for the soil moisture trends in all considered reanalyses – not just ERA5/ERA5-Land, for which this is expected due the model internal consistency – and in most of the satellite-based products (Fig. B1 of the Appendix A). On the contrary, the soil moisture trends in ESA-CCI-ACT are mixed for all aridity trend regimes, consistently with the weaker drought representation found for this product (Fig. 9). As argued, trends in vegetation cover or density may reflect in the soil moisture signal of the remote sensing products for the role they play in the uncertainty budget, but should also reflect the soil moisture signal as a result of changes in water availability in both satellite and model data. In the case of tree cover (Fig. B2), ESA-CCI-ACT shows a relation with (dry) wet trends in areas of (de-)forestation, while ESA-CCI-PAS shows the opposite relation. A positive relation is to a lesser extent also visible in ERA5/ERA5-Land (more pronounced in the root zone) and ESA-CCI-COM-RZSM (when considering q75 of the trend distributions) as well as in MERRA-2 (when considering q25). Conversely, global VOD (Fig. B3) only explains trends in the ESA-CCI-ACT product and to a lesser extent in ESA-CCI-COM and -RZSM, but does not relate to the modelled trends, neither in the surface nor in the root zone. The physical relation between VOD and water availability shows more clearly when water limited areas only are considered (below the 25th percentile of the mean ERA5 100–289 cm depth layer soil moisture for the 2000–2020 period, Fig. B4). In this case, soil moisture emerges more distinctly as a vegetation control in the remote sensing products (Lyons et al., 2021), and is better captured by the satellite-based products. No distinct relations emerge with bare soil trends for either of the products (if not a mild negative relation to ERA5/ERA5-Land trends), although

a subsurface scattering effect (Wagner et al., 2022) might explain remarkably wetter trends in the higher bare ground
720 quantiles for ESA-CCI-ACT (Fig. B5). ESA-CCI-ACT also displays an evident increase in soil moisture trends with trends
of urban area fraction (Fig. B6). This is consistent with similar observations made for the ASCAT-derived products (Hahn et
al., 2023), and visible also in ESA-CCI-COM (which also ingest ASCAT).

In synthesis, several controls can be identified for the soil moisture trends in the various products, although no one variable
725 explains all trends coherently. In some cases (e.g., for urban area), these may be artifacts of the L0 signal that should be
decoupled in the retrieval of soil moisture through an update in the model parametrisation. In other cases, it is reasonable to
assume some form of relationship (e.g., for the aridity indicator or for VOD in water-limited regions), which, however, a few
products fail to render.

6 Conclusions

730 We investigated the potential of long-term remote-sensing and selected state-of-the-art reanalysis products for characterising
soil drying by analysing their 2000–2022 Theil-Sen soil moisture trends and their ability to capture major agroecological
drought events of this period. The product differences in the representation of the drought events as a use case were
confronted with the soil moisture trends and their drivers, and a synthesis of the global trends was provided based on the
best-estimate products. We focused on the relative behaviour of the products to circumvent the lack of widely available
735 ground data of soil moisture. Thus, we did not aim for an in situ validation of the products regarding their representation of
the soil moisture trends and considered drought events but focused on the product ensemble and identify the products with
larger deviations from the majority to collect convergence of evidence.

Global distributions of the soil moisture trends are diverse and partly contradictory between the products. ERA5-Land,
740 ERA5 and ESA-CCI-COM show larger area fractions of drying trends in surface soil moisture, while ESA-CCI-ACT and
MERRA-2 show larger fractions of wetting trends (with area fractions of approximately 60 % and above in both cases).
Also, corresponding trend magnitudes diverge, resulting in global mean wetting trends for ESA-CCI-ACT and MERRA-2,
while all other products show global mean drying trends. The different global patterns of soil moisture trends of the
reanalysis products ERA5/ERA5-Land and MERRA-2 are reflected in regional differences in their runoff and particular
745 evapotranspiration trends. These differences are driven by a positive mean bias in the precipitation trends of MERRA-2 and
a larger RMSD compared to ERA5, which has a slight negative bias and a lower RMSD compared to observed precipitation
trends (0.171 vs. -0.004 mm d⁻¹ (20 yr)⁻¹ bias and 0.847 vs. 0.492 mm d⁻¹ (20 yr)⁻¹ RMSD of MERRA-2 compared to
ERA5). The diverse soil moisture and evapotranspiration trends also show a clear link to regional differences in 2 m
temperature trends in parts of Asia, Africa, and North America, where MERRA-2 shows a negative bias compared to
750 observed temperature trends, and a corresponding larger RMSD than ERA5/ERA5-Land (0.613 K (20 yr)⁻¹ RMSD of

MERRA-2 compared to $0.536 \text{ K (20 yr)}^{-1}$ of ERA5 respectively $0.511 \text{ K (20 yr)}^{-1}$ of ERA5-Land). The lower bias in precipitation trends of ERA5 and its stronger constraint with observed regional temperature trends results in more widespread soil moisture drying and evapotranspiration decreases of ERA5/ERA5-Land. In MERRA-2, the too strong positive trends in precipitation translate into more widespread wetting trends in soil moisture and enhanced evapotranspiration, and an unrealistic regional cooling.

Given these biases in MERRA-2 precipitation and temperature trends, but also based on available validation studies, ESA-CCI-COM and -RZSM, as well as ERA5-Land were considered for a synthesis of global surface and root zone soil moisture trends. Based on these best-estimate products, common soil moisture drying trends can be observed in 49.3% of the surface and 44.5% of the root zone layers of the covered global area. The common drying trends are localized in Siberia, in the region of the Black Sea/Caspian Sea and Central Asia, in parts of Europe and the Mediterranean, parts of western USA and the Canadian Prairies, as well as larger parts of South America, parts of southern and northern Africa and northwest Australia.

We also analysed the products' ability to detect major drought events as a use case based on their severity, magnitude, duration, and spatial extent, which are calculated from standardised daily anomalies of surface and root zone soil moisture. We considered well documented drought events selected based on scientific literature and drought reports. The investigated products mostly capture the considered 17 drought events. The ESA-CCI-ACT microwave remote-sensing, and to a lesser extent the ESA-CCI-PAS products, tend to show partly weaker drought signals based on surface soil moisture in all metrics compared to the combined ESA-CCI-COM product and ERA5/ERA5-Land. This is most pronounced for the drought magnitudes of ESA-CCI-ACT. The magnitudes are also reduced in MERRA-2 both in the surface layer and the root zone. ESA-CCI-COM displays partly stronger drought severities and prolonged durations. In the root zone (based on the reanalysis products and ESA-CCI-COM-RZSM), the drought events appear dampened in magnitude and smaller in spatial extent, while a tendency to prolonged durations and stronger severities of the droughts is observable (except for MERRA-2). ESA-CCI-COM-RZSM displays partly stronger representation of the droughts in severity and magnitude compared to the reanalysis products.

The product deviations in drought magnitude and severity further showed a significant relation with deviations in the soil moisture trends in areas without trend direction agreement. This is most visible in the reduced drought magnitudes of MERRA-2 and the ESA-CCI-ACT remote sensing product compared to the other products, which is linked to their larger global fractions of strong positive trends in soil moisture. In areas with drying trend agreement of the products, however, such a relation between product deviations in the drought magnitude and severity, and the corresponding deviations in the trend was not present. This study demonstrates that soil moisture trends play a fundamental role for the drought-detection capacity of different products. Uncertainties in the representation and global distribution of soil moisture trends, as reflected

785 in the large proportions of areas where there is no consensus in trend direction, both between and among remote sensing and reanalysis products, contribute to product-specific representations of droughts, particularly affecting the drought magnitude.

We also identified several land-surface characteristics and bioclimatic indicators (i.e., aridity, VOD, fractional coverage of urban area, of tree cover and of bare soil) that control soil moisture trends in the various products, although none of these explains all trends coherently. The analysis of trends in these land-surface and bioclimatic variables qualitatively showed that the soil moisture trends are affected by retrieval or modelling artifacts, e.g., due to non-valid stationarity assumptions in the land-surface variables. Conversely, trends in these variables may show valid physical relationships to trends in soil moisture (e.g., in case of aridity, VOD in water-limited regions), which are however not represented by some products. As a future step, the exact sources of such artifacts should be identified to reconcile the different – and partially diverging – trends representations and advance the drought assessment capacity of the remote sensing observations and reanalysis systems.

790
795

Appendix A

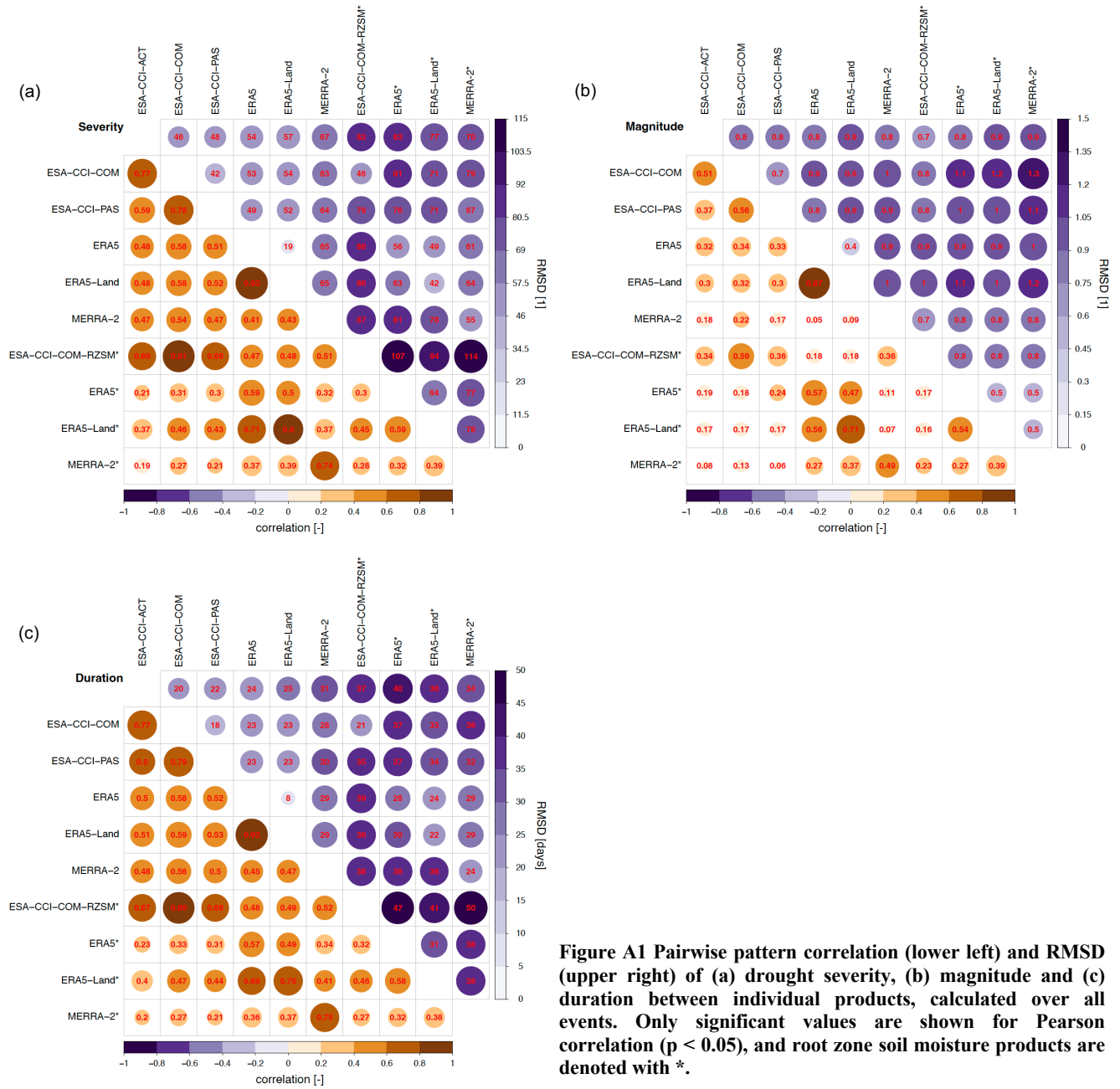


Figure A1 Pairwise pattern correlation (lower left) and RMSD (upper right) of (a) drought severity, (b) magnitude and (c) duration between individual products, calculated over all events. Only significant values are shown for Pearson correlation ($p < 0.05$), and root zone soil moisture products are denoted with *.

Appendix B

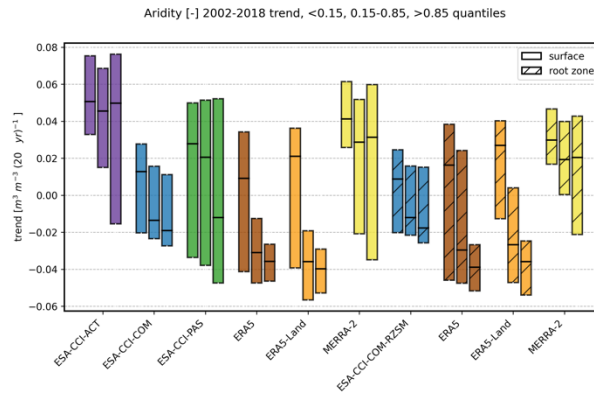
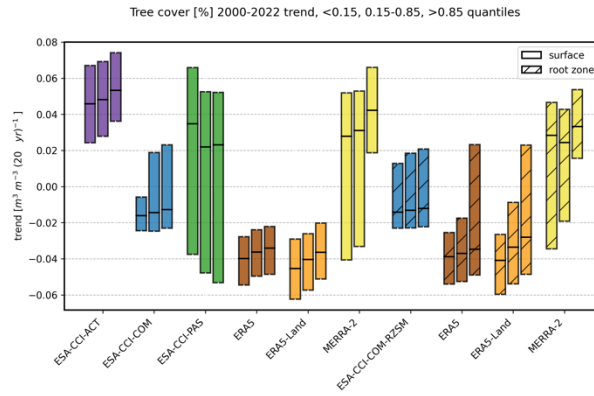


Figure B1 Distributions (median, inter-quartile range) of global soil moisture trends in the different products in relation to different quantile bins of trends in aridity (i.e., <0.15, 0.15-0.85, >0.85). Note that trends are not masked for significance.



805

Figure B2 As Fig. B1, but for trends in tree cover fraction.

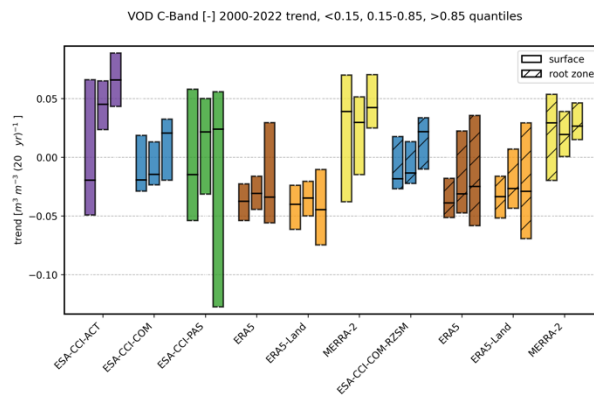
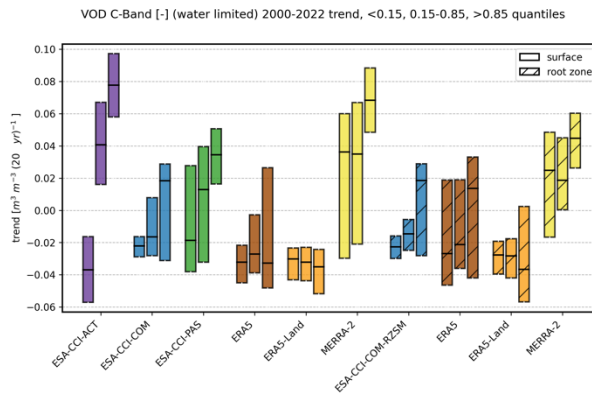


Figure B3 As Fig. B1, but for trends in global VOD.



810

Figure B4 As Fig. B1, but for trends VOD in water-limited regions.

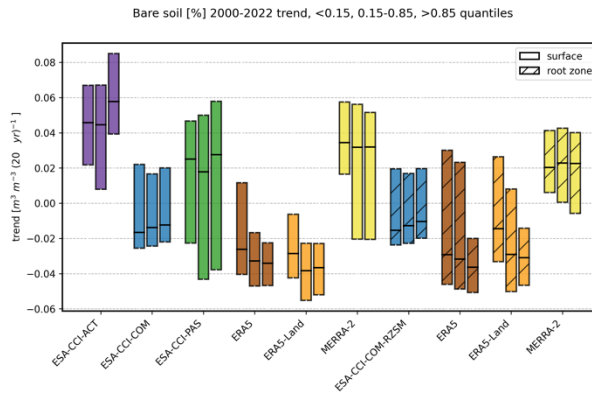
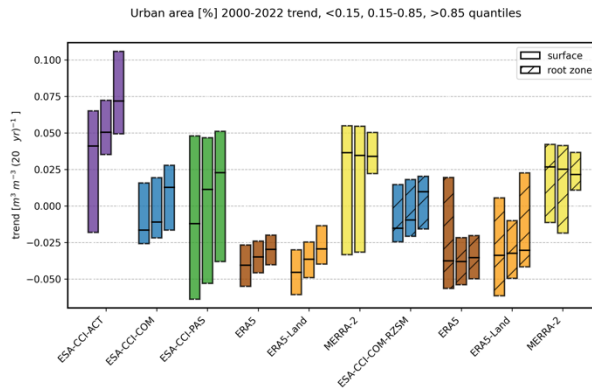


Figure B5 As Fig. B1, but for trends in bare soil fraction.



815 Figure B6 As Fig. B1, but for trends in urban area fraction.

Author contribution

MH, PS, BC, WD and SIS: Conceptualization; MH, BC, PS: Formal analysis, Investigation, Methodology, Visualization; MH: Writing – original draft preparation; all authors: Writing – review & editing.

Competing interests

820 The authors declare that they have no conflict of interest.

Acknowledgements

M.H., P.S. and W.D. acknowledge financial support by the ESA's Climate Change Initiative for Soil Moisture (Contract No. 4000126684/19/I-NB). The authors acknowledge the Copernicus Climate Change Service C3S_511 which is being funded by the European Union and Implemented by ECMWF.

825 References

- Albergel, C., Dorigo, W., Reichle, R. H., Balsamo, G., de Rosnay, P., Munoz-Sabater, J., Isaksen, L., de Jeu, R., and Wagner, W.: Skill and Global Trend Analysis of Soil Moisture from Reanalyses and Microwave Remote Sensing, *Journal of Hydrometeorology*, 14, 1259-1277, 10.1175/jhm-d-12-0161.1, 2013.
- Albergel, C., Rüdiger, C., Pellarin, T., Calvet, J. C., Fritz, N., Froissard, F., Suquia, D., Petitpa, A., Pignatelli, B., and Martin,
830 E.: From near-surface to root-zone soil moisture using an exponential filter: an assessment of the method based on in-situ observations and model simulations, *Hydrology and Earth System Sciences*, 12, 1323-1337, 10.5194/hess-12-1323-2008, 2008.
- An, R., Zhang, L., Wang, Z., Quaye-Ballard, J. A., You, J. J., Shen, X. J., Gao, W., Huang, L. J., Zhao, Y. H., and Ke, Z. Y.: Validation of the ESA CCI soil moisture product in China, *Int J Appl Earth Obs*, 48, 28-36, 10.1016/j.jag.2015.09.009, 2016.
- 835 Balsamo, G., Viterbo, P., Beljaars, A., van den Hurk, B., Hirschi, M., Betts, A. K., and Scipal, K.: A Revised Hydrology for the ECMWF Model: Verification from Field Site to Terrestrial Water Storage and Impact in the Integrated Forecast System, *Journal of Hydrometeorology*, 10, 623-643, 10.1175/2008jhm1068.1, 2009.
- Beck, H. E., Pan, M., Miralles, D. G., Reichle, R. H., Dorigo, W. A., Hahn, S., Sheffield, J., Karthikeyan, L., Balsamo, G., Parinussa, R. M., van Dijk, A. I. J. M., Du, J. Y., Kimball, J. S., Vergopolan, N., and Wood, E. F.: Evaluation of 18 satellite-
840 and model-based soil moisture products using in situ measurements from 826 sensors, *Hydrology and Earth System Sciences*, 25, 17-40, 10.5194/hess-25-17-2021, 2021.
- Bosilovich, M. G., Akella, S., Coy, L., Cullather, R., Draper, C., Gelaro, R., Kovach, R., Liu, Q., Molod, A., Norris, P., Wargan, K., Chao, W., Reichle, R., Takacs, L., Vikhliayev, Y., Bloom, S., Collon, A., Firth, S., Labow, G., Partyka, G.,

- Pawson, S., Reale, O., Schubert, S. D., and Suarez, M.: MERRA-2: Initial evaluation of the climate, National Aeronautics and Space Administration, Goddard Space Flight Center, Greenbelt, Maryland, <https://gmao.gsfc.nasa.gov/pubs/docs/Bosilovich803.pdf>, 15-09-2023, 2015.
- Bueechi, E., Fischer, M., Crocetti, L., Trnka, M., Grlj, A., Zappa, L., and Dorigo, W.: Crop yield anomaly forecasting in the Pannonian basin using gradient boosting and its performance in years of severe drought, *Agricultural and Forest Meteorology*, 340, 10.1016/j.agrformet.2023.109596, 2023.
- 850 C3S: Land cover classification gridded maps from 1992 to present derived from satellite observation, Copernicus Climate Change Service (C3S) Climate Data Store (CDS) [dataset], 10.24381/cds.006f2c9a 2019.
- Champagne, C., White, J., Berg, A., Belair, S., and Carrera, M.: Impact of Soil Moisture Data Characteristics on the Sensitivity to Crop Yields Under Drought and Excess Moisture Conditions, *Remote Sensing*, 11, ARTN 372 10.3390/rs11040372, 2019.
- 855 Cheng, S. J., Guan, X. D., Huang, J. P., Ji, F., and Guo, R. X.: Long-term trend and variability of soil moisture over East Asia, *Journal of Geophysical Research-Atmospheres*, 120, 8658-8670, 10.1002/2015jd023206, 2015.
- Crezee, B., Hirschi, M., Thorne, P., Coll, J., Müller, B., Yang, C., Pisano, A., and Hassler, B.: Deliverable D511.1.5: Data catalogue for extreme events and extreme event metrics, online, 54, <https://drive.google.com/file/d/13KIOW-1xq82LuMKLvbS2MmOtCDMMpYWO/view>, 15-09-2023, 2019.
- 860 de Rosnay, P., Balsamo, G., Albergel, C., Munoz-Sabater, J., and Isaksen, L.: Initialisation of Land Surface Variables for Numerical Weather Prediction, *Surv Geophys*, 35, 607-621, 10.1007/s10712-012-9207-x, 2014.
- de Rosnay, P., Drusch, M., Vasiljevic, D., Balsamo, G., Albergel, C., and Isaksen, L.: A simplified Extended Kalman Filter for the global operational soil moisture analysis at ECMWF, *Quarterly Journal of the Royal Meteorological Society*, 139, 1199-1213, 10.1002/qj.2023, 2013.
- 865 Dirmeyer, P. A., Wu, J. X., Norton, H. E., Dorigo, W. A., Quiring, S. M., Ford, T. W., Santanello, J. A., Bosilovich, M. G., Ek, M. B., Koster, R. D., Balsamo, G., and Lawrence, D. M.: Confronting Weather and Climate Models with Observational Data from Soil Moisture Networks over the United States, *Journal of Hydrometeorology*, 17, 1049-1067, 10.1175/Jhm-D-15-0196.1, 2016.
- Dorigo, W., de Jeu, R., Chung, D., Parinussa, R., Liu, Y., Wagner, W., and Fernandez-Prieto, D.: Evaluating global trends (1988-2010) in harmonized multi-satellite surface soil moisture, *Geophysical Research Letters*, 39, 10.1029/2012gl052988, 2012.
- 870 Dorigo, W., Preimesberger, W., Hahn, S., Van der Schalie, R., De Jeu, R., Kidd, R., Rodriguez-Fernandez, N., Hirschi, M., Stradiotti, P., Frederikse, T., Gruber, A., and Madelon, R.: ESA Soil Moisture Climate Change Initiative (Soil_Moisture_cci): Version 08.1 data collection., NERC EDS Centre for Environmental Data Analysis [dataset], <http://catalogue.ceda.ac.uk/uuid/ff890589c21f4033803aa550f52c980c>, 26-08-2023, 2023.
- 875

- Dorigo, W., Preimesberger, W., Moesinger, L., Pasik, A., Scanlon, T., Hahn, S., Van der Schalie, R., Van der Vliet, M., De Jeu, R., Kidd, R., Rodriguez-Fernandez, N., and Hirschi, M.: ESA Soil Moisture Climate Change Initiative (Soil_Moisture_cci): Version 06.1 data collection [dataset], 10.5285/28935552223242ca97953a8db99c2821, 2021a.
- 880 Dorigo, W., Wagner, W., Albergel, C., Albrecht, F., Balsamo, G., Brocca, L., Chung, D., Ertl, M., Forkel, M., Gruber, A., Haas, E., Hamer, P. D., Hirschi, M., Ikonen, J., de Jeu, R., Kidd, R., Lahoz, W., Liu, Y. Y., Miralles, D., Mistelbauer, T., Nicolai-Shaw, N., Parinussa, R., Pratola, C., Reimer, C., van der Schalie, R., Seneviratne, S. I., Smolander, T., and Lecomte, P.: ESA CCI Soil Moisture for improved Earth system understanding: State-of-the art and future directions, *Remote Sensing of Environment*, 203, 185-215, 10.1016/j.rse.2017.07.001, 2017.
- 885 Dorigo, W., Himmelbauer, I., Aberer, D., Schremmer, L., Petrakovic, I., Zappa, L., Preimesberger, W., Xaver, A., Annor, F., Ardö, J., Baldocchi, D., Bitelli, M., Blöschl, G., Boga, H., Brocca, L., Calvet, J. C., Camarero, J. J., Capello, G., Choi, M., Cosh, M. C., van de Giesen, N., Hajdu, I., Ikonen, J., Jensen, K. H., Kanniah, K. D., de Kat, I., Kirchengast, G., Kumar Rai, P., Kyrouac, J., Larson, K., Liu, S., Loew, A., Moghaddam, M., Martínez Fernández, J., Mattar Bader, C., Morbidelli, R., Musial, J. P., Osenga, E., Palecki, M. A., Pellarin, T., Petropoulos, G. P., Pfeil, I., Powers, J., Robock, A., Rüdiger, C., Rummel, U., Strobel, M., Su, Z., Sullivan, R., Tagesson, T., Varlagin, A., Vreugdenhil, M., Walker, J., Wen, J., Wenger, F.,
- 890 Wigneron, J. P., Woods, M., Yang, K., Zeng, Y., Zhang, X., Zreda, M., Dietrich, S., Gruber, A., van Oevelen, P., Wagner, W., Scipal, K., Drusch, M., and Sabia, R.: The International Soil Moisture Network: serving Earth system science for over a decade, *Hydrol. Earth Syst. Sci.*, 25, 5749-5804, 10.5194/hess-25-5749-2021, 2021b.
- Dorigo, W. A., Gruber, A., De Jeu, R. A. M., Wagner, W., Stacke, T., Loew, A., Albergel, C., Brocca, L., Chung, D., Parinussa, R. M., and Kidd, R.: Evaluation of the ESA CCI soil moisture product using ground-based observations, *Remote*
- 895 *Sensing of Environment*, 162, 380-395, 10.1016/j.rse.2014.07.023, 2015.
- Dorigo, W. A., Wagner, W., Hohensinn, R., Hahn, S., Paulik, C., Xaver, A., Gruber, A., Drusch, M., Mecklenburg, S., van Oevelen, P., Robock, A., and Jackson, T.: The International Soil Moisture Network: a data hosting facility for global in situ soil moisture measurements, *Hydrology and Earth System Sciences*, 15, 1675-1698, 10.5194/hess-15-1675-2011, 2011.
- 900 Douville, H., Raghavan, K., Renwick, J., Allan, R. P., Arias, P. A., Barlow, M., Cerezo-Mota, R., Cherchi, A., Gan, T. Y., Gergis, J., Jiang, D., Khan, A., Mba, W. P., Rosenfeld, D., Tierney, J., and Zolina, O.: Water Cycle Changes, in: *Climate Change 2021: The Physical Science Basis. Contribution of Working Group I to the Sixth Assessment Report of the Intergovernmental Panel on Climate Change*, edited by: Masson-Delmotte, V., Zhai, P., Pirani, A., Connors, S. L., Péan, C., Berger, S., Caud, N., Chen, Y., Goldfarb, L., Gomis, M. I., Huang, M., Leitzell, K., Lonnoy, E., Matthews, J. B. R., Maycock, T. K., Waterfield, T., Yelekçi, O., Yu, R., and Zhou, B., Cambridge University Press, 1055–1210,
- 905 10.1017/9781009157896.010, 2021.
- Fairbairn, D., de Rosnay, P., and Browne, P. A.: The New Stand-Alone Surface Analysis at ECMWF: Implications for Land-Atmosphere DA Coupling, *Journal of Hydrometeorology*, 20, 2023-2042, 10.1175/Jhm-D-19-0074.1, 2019.
- Feng, H. H. and Zhang, M. Y.: Global land moisture trends: drier in dry and wetter in wet over land, *Sci Rep-Uk*, 5, ARTN 18018

910 10.1038/srep18018, 2015.

Fennig, K., Schroder, M., Andersson, A., and Hollmann, R.: A Fundamental Climate Data Record of SMMR, SSM/I, and SSMIS brightness temperatures, *Earth System Science Data*, 12, 647-681, 10.5194/essd-12-647-2020, 2020.

GCOS: The global observing system for climate: Implementation needs GCOS-200, 2016.

Gelaro, R., McCarty, W., Suarez, M. J., Todling, R., Molod, A., Takacs, L., Randles, C. A., Darmenov, A., Bosilovich, M.,
915 G., Reichle, R., Wargan, K., Coy, L., Cullather, R., Draper, C., Akella, S., Buchard, V., Conaty, A., da Silva, A. M., Gu, W.,
Kim, G.-K., Koster, R., Lucchesi, R., Merkova, D., Nielsen, J. E., Partyka, G., Pawson, S., Putman, W., Rienecker, M.,
Schubert, S. D., Sienkiewicz, M., and Zhao, B.: The Modern-Era Retrospective Analysis for Research and Applications,
Version 2 (MERRA-2), *Journal of Climate*, 30, 5419-5454, 10.1175/jcli-d-16-0758.1, 2017.

GMAO: MERRA-2 tavg1_2d_lnd_Nx: 2d,1-Hourly,Time-Averaged,Single-Level,Assimilation,Land Surface Diagnostics
920 V5.12.4 [dataset], 10.5067/RKPHT8KC1Y1T, 2015.

Gruber, A., Scanlon, T., van der Schalie, R., Wagner, W., and Dorigo, W.: Evolution of the ESA CCI Soil Moisture climate
data records and their underlying merging methodology, *Earth System Science Data*, 11, 717-739, 10.5194/essd-11-717-
2019, 2019.

Gu, X. H., Li, J. F., Chen, Y. D., Kong, D. D., and Liu, J. Y.: Consistency and Discrepancy of Global Surface Soil Moisture
925 Changes From Multiple Model-Based Data Sets Against Satellite Observations, *Journal of Geophysical Research-
Atmospheres*, 124, 1474-1495, 10.1029/2018jd029304, 2019.

Gudmundsson, L., Rego, F. C., Rocha, M., and Seneviratne, S. I.: Predicting above normal wildfire activity in southern
Europe as a function of meteorological drought, *Environ Res Lett*, 9, 10.1088/1748-9326/9/8/084008, 2014.

H SAF: Algorithm Theoretical Baseline Document (ATBD) Metop ASCAT Surface Soil Moisture Climate Data Record v7
930 12.5 km sampling (H119) and extension (H120), v0.1, 2021.

Hahn, S., Wagner, W., Alves, O., Muguda Sanjeevamurthy, P., Vreugdenhil, M., and Melzer, T.: Metop ASCAT soil
moisture trends: Mitigating the effects of long-term land cover changes, *EGU General Assembly 2023*, Vienna,
10.5194/egusphere-egu23-16205, 2023.

Hanel, M., Rakovec, O., Markonis, Y., Maca, P., Samaniego, L., Kysely, J., and Kumar, R.: Revisiting the recent European
935 droughts from a long-term perspective, *Sci Rep-Uk*, 8, 10.1038/s41598-018-27464-4, 2018.

Harris, I., Osborn, T. J., Jones, P., and Lister, D.: Version 4 of the CRU TS monthly high-resolution gridded multivariate
climate dataset, *Scientific Data*, 7, ARTN 109
10.1038/s41597-020-0453-3, 2020.

He, Q., Lu, H., and Yang, K.: Soil Moisture Memory of Land Surface Models Utilized in Major Reanalyses Differ
940 Significantly From SMAP Observation, *Earths Future*, 11, 10.1029/2022EF003215, 2023.

Hersbach, H., Bell, B., Berrisford, P., Hirahara, S., Horányi, A., Muñoz-Sabater, J., Nicolas, J., Peubey, C., Radu, R.,
Schepers, D., Simmons, A., Soci, C., Abdalla, S., Abellan, X., Balsamo, G., Bechtold, P., Biavati, G., Bidlot, J., Bonavita,
M., De Chiara, G., Dahlgren, P., Dee, D., Diamantakis, M., Dragani, R., Flemming, J., Forbes, R., Fuentes, M., Geer, A.,

- Haimberger, L., Healy, S., Hogan, R. J., Hólm, E., Janisková, M., Keeley, S., Laloyaux, P., Lopez, P., Lupu, C., Radnoti, G.,
945 de Rosnay, P., Rozum, I., Vamborg, F., Villaume, S., and Thépaut, J.-N.: The ERA5 Global Reanalysis, *Quarterly Journal of
the Royal Meteorological Society*, 10.1002/qj.3803, 2020.
- Hirschi, M., Mueller, B., Dorigo, W., and Seneviratne, S. I.: Using remotely sensed soil moisture for land-atmosphere
coupling diagnostics: The role of surface vs. root-zone soil moisture variability, *Remote Sensing of Environment*, 154, 246-
252, 10.1016/j.rse.2014.08.030, 2014.
- 950 Hirschi, M., Stradiotti, P., Preimesberger, W., Dorigo, W., and Kidd, R.: Product Validation and Intercomparison Report
(PVIR): Supporting Product version v08.1. Deliverable D4.1 Version 1, ESA Climate Change Initiative Plus - Soil Moisture,
10.5281/zenodo.8320930, 2023.
- Hirschi, M., Seneviratne, S. I., Alexandrov, V., Boberg, F., Boroneant, C., Christensen, O. B., Formayer, H., Orłowsky, B.,
and Stepanek, P.: Observational evidence for soil-moisture impact on hot extremes in southeastern Europe, *Nat Geosci*, 4,
955 17-21, 10.1038/Ngeo1032, 2011.
- Jia, B. H., Liu, J. G., Xie, Z. H., and Shi, C. X.: Interannual Variations and Trends in Remotely Sensed and Modeled Soil
Moisture in China, *Journal of Hydrometeorology*, 19, 831-847, 10.1175/Jhm-D-18-0003.1, 2018.
- Koster, R. D., Mahanama, S. P. P., Livneh, B., Lettenmaier, D. P., and Reichle, R. H.: Skill in streamflow forecasts derived
from large-scale estimates of soil moisture and snow, *Nat Geosci*, 3, 613-616, 10.1038/Ngeo944, 2010.
- 960 Koster, R. D., Suarez, M. J., Ducharne, A., Stieglitz, M., and Kumar, P.: A catchment-based approach to modeling land
surface processes in a general circulation model: 1. Model structure, *Journal of Geophysical Research: Atmospheres*, 105,
24809-24822, 10.1029/2000jd900327, 2000.
- Koster, R. D., Guo, Z., Yang, R., Dirmeyer, P. A., Mitchell, K., and Puma, M. J.: On the Nature of Soil Moisture in Land
Surface Models, *Journal of Climate*, 22, 4322-4335, 10.1175/2009jcli2832.1, 2009.
- 965 Li, M., Wu, P., and Ma, Z.: A comprehensive evaluation of soil moisture and soil temperature from third-generation
atmospheric and land reanalysis data sets, *International Journal of Climatology*, 40, 5744-5766, 10.1002/joc.6549, 2020.
- Li, X. W., Gao, X. Z., Wang, J. K., and Guoa, H. D.: Microwave soil moisture dynamics and response to climate change in
Central Asia and Xinjiang Province, China, over the last 30 years, *Journal of Applied Remote Sensing*, 9, Artn 096012
10.1117/1.Jrs.9.096012, 2015.
- 970 Liu, L. B., Gudmundsson, L., Hauser, M., Qin, D. H., Li, S. C., and Seneviratne, S. I.: Soil moisture dominates dryness stress
on ecosystem production globally, *Nature Communications*, 11, 10.1038/s41467-020-18631-1, 2020.
- Lloyd-Hughes, B. and Saunders, M. A.: A drought climatology for Europe, *International Journal of Climatology*, 22, 1571-
1592, 10.1002/joc.846, 2002.
- Loew, A., Stacke, T., Dorigo, W., de Jeu, R., and Hagemann, S.: Potential and limitations of multidecadal satellite soil
975 moisture observations for selected climate model evaluation studies, *Hydrology and Earth System Sciences*, 17, 3523-3542,
10.5194/hess-17-3523-2013, 2013.

- Lyons, D. S., Dobrowski, S. Z., Holden, Z. A., Maneta, M. P., and Sala, A.: Soil moisture variation drives canopy water content dynamics across the western US, *Remote Sensing of Environment*, 253, 10.1016/j.rse.2020.112233, 2021.
- 980 McKee, T. B., Doesken, N. J., and Kleist, J.: The relationship of drought frequency and duration to time scales, Anaheim, California, USA, 17--22 January, 1993.
- Miralles, D. G., Teuling, A. J., van Heerwaarden, C. C., and Vila-Guerau de Arellano, J.: Mega-heatwave temperatures due to combined soil desiccation and atmospheric heat accumulation, *Nat Geosci*, 7, 345--349, 10.1038/ngeo2141, 2014.
- Moravec, V., Markonis, Y., Rakovec, O., Kumar, R., and Hanel, M.: A 250-Year European Drought Inventory Derived From Ensemble Hydrologic Modeling, *Geophysical Research Letters*, 46, 5909-5917, 10.1029/2019gl082783, 2019.
- 985 Mueller, B. and Seneviratne, S. I.: Hot days induced by precipitation deficits at the global scale, *Proceedings of the National Academy of Sciences*, 109, 12398-12403, 10.1073/pnas.1204330109, 2012.
- Muñoz-Sabater, J., Dutra, E., Agustí-Panareda, A., Albergel, C., Arduini, G., Balsamo, G., Boussetta, S., Choulga, M., Harrigan, S., Hersbach, H., Martens, B., Miralles, D. G., Piles, M., Rodríguez-Fernández, N. J., Zsoter, E., Buontempo, C., and Thépaut, J.-N.: ERA5-Land: a state-of-the-art global reanalysis dataset for land applications, *Earth Syst. Sci. Data*, 13, 990 4349-4383, 10.5194/essd-13-4349-2021, 2021.
- Naeimi, V., Scipal, K., Bartalis, Z., Hasenauer, S., and Wagner, W.: An Improved Soil Moisture Retrieval Algorithm for ERS and METOP Scatterometer Observations, *Ieee Transactions on Geoscience and Remote Sensing*, 47, 1999-2013, 10.1109/Tgrs.2008.2011617, 2009.
- Orlowsky, B. and Seneviratne, S. I.: Elusive drought: uncertainty in observed trends and short- and long-term CMIP5 995 projections, *Hydrology and Earth System Sciences*, 17, 1765-1781, 10.5194/hess-17-1765-2013, 2013.
- Padron, R. S., Gudmundsson, L., Decharme, B., Ducharne, A., Lawrence, D. M., Mao, J. F., Peano, D., Krinner, G., Kim, H., and Seneviratne, S. I.: Observed changes in dry-season water availability attributed to human-induced climate change, *Nat Geosci*, 13, 477+, 10.1038/s41561-020-0594-1, 2020.
- Pasik, A., Gruber, A., Preimesberger, W., De Santis, D., and Dorigo, W.: Uncertainty estimation for a new exponential filter- 1000 based long-term root-zone soil moisture dataset from C3S surface observations, *EGUsphere*, 2023, 1-32, 10.5194/egusphere-2023-47, 2023.
- Preimesberger, W., Scanlon, T., Su, C.-H., Gruber, A., and Dorigo, W.: Homogenization of Structural Breaks in the Global ESA CCI Soil Moisture Multisatellite Climate Data Record, *IEEE Transactions on Geoscience and Remote Sensing*, 59, 2845-2862, 10.1109/tgrs.2020.3012896, 2021.
- 1005 Qiu, J. X., Gao, Q. Z., Wang, S., and Su, Z. R.: Comparison of temporal trends from multiple soil moisture data sets and precipitation: The implication of irrigation on regional soil moisture trend, *Int J Appl Earth Obs*, 48, 17-27, 10.1016/j.jag.2015.11.012, 2016.
- Rahmani, A., Golian, S., and Brocca, L.: Multiyear monitoring of soil moisture over Iran through satellite and reanalysis soil moisture products, *Int J Appl Earth Obs*, 48, 85-95, 10.1016/j.jag.2015.06.009, 2016.

- 1010 Reichle, R. H., Liu, Q., Koster, R. D., Draper, C. S., Mahanama, S. P. P., and Partyka, G. S.: Land Surface Precipitation in MERRA-2, *Journal of Climate*, 30, 1643-1664, 10.1175/jcli-d-16-0570.1, 2017a.
- Reichle, R. H., Draper, C. S., Liu, Q., Giroto, M., Mahanama, S. P. P., Koster, R. D., and De Lannoy, G. J. M.: Assessment of MERRA-2 Land Surface Hydrology Estimates, *Journal of Climate*, 30, 2937-2960, 10.1175/jcli-d-16-0720.1, 2017b.
- Rodell, M., Houser, P. R., Jambor, U., Gottschalck, J., Mitchell, K., Meng, C. J., Arsenault, K., Cosgrove, B., Radakovich, J., Bosilovich, M., Entin, J. K., Walker, J. P., Lohmann, D., and Toll, D.: The global land data assimilation system, *Bulletin of the American Meteorological Society*, 85, 381–394 10.1175/Bams-85-3-381, 2004.
- 1015 Saxton, K. E. and Rawls, W. J.: Soil water characteristic estimates by texture and organic matter for hydrologic solutions, *Soil Sci Soc Am J*, 70, 1569-1578, 10.2136/sssaj2005.0117, 2006.
- Scherrer, S. C., Hirschi, M., Spirig, C., Maurer, F., and Kotlarski, S.: Trends and drivers of recent summer drying in Switzerland, *Environmental Research Communications*, 4, 10.1088/2515-7620/ac4fb9, 2022.
- 1020 Schumacher, D. L., Zachariah, M., Otto, F., Barnes, C., Philip, S., Kew, S., Vahlberg, M., Singh, R., Heinrich, D., Arrighi, J., van Aalst, M., Hauser, M., Hirschi, M., Bessenbacher, V., Gudmundsson, L., Beaudoin, H. K., Rodell, M., Li, S. H., Yang, W. C., Vecchi, G. A., Harrington, L. J., Lehner, F., Balsamo, G., and Seneviratne, S. I.: Detecting the human fingerprint in the summer 2022 western-central European soil drought, *Earth System Dynamics*, 15, 131-154, 10.5194/esd-1025 15-131-2024, 2024.
- Schumacher, D. L., Zachariah, M., Otto, F., Barnes, C., Philip, S., Kew, S., Vahlberg, M., Singh, R., Heinrich, D., Arrighi, J., Aalst, M. v., Thalheimer, L., Raju, E., Hauser, M., Hirschi, M., Gudmundsson, L., Beaudoin, H. K., Rodell, M., Li, S., Yang, W., Vecchi, G. A., Vautard, R., Harrington, L. J., and Seneviratne, S. I.: High temperatures exacerbated by climate change made 2022 Northern Hemisphere soil moisture droughts more likely, *World Weather Attribution*, 10.1038/491338a, 2022.
- 1030 <https://www.worldweatherattribution.org/wp-content/uploads/WCE-NH-drought-scientific-report.pdf>, 15-09-2023, 2022.
- Schwingshackl, C., Hirschi, M., and Seneviratne, S. I.: Quantifying Spatiotemporal Variations of Soil Moisture Control on Surface Energy Balance and Near-Surface Air Temperature, *Journal of Climate*, 30, 7105-7124, 10.1175/Jcli-D-16-0727.1, 2017.
- Seneviratne, S. I.: Climate science: Historical drought trends revisited, *Nature*, 491, 338--339, 10.1038/491338a, 2012.
- 1035 Seneviratne, S. I., Corti, T., Davin, E. L., Hirschi, M., Jaeger, E. B., Lehner, I., Orlowsky, B., and Teuling, A. J.: Investigating soil moisture-climate interactions in a changing climate: A review, *Earth-Sci Rev*, 99, 125-161, 10.1016/j.earscirev.2010.02.004, 2010.
- Seneviratne, S. I., Zhang, X., Adnan, M., Badi, W., Dereczynski, C., Luca, A. D., Ghosh, S., Iskandar, I., Kossin, J., Lewis, S., Otto, F., Pinto, I., Satoh, M., Vicente-Serrano, S. M., Wehner, M., and Zhou, B.: Weather and Climate Extreme Events in a Changing Climate, in: *Climate Change 2021: The Physical Science Basis. Contribution of Working Group I to the Sixth Assessment Report of the Intergovernmental Panel on Climate Change*, edited by: Masson-Delmotte, V., Zhai, P., Pirani, A., Connors, S. L., Péan, C., Berger, S., Caud, N., Chen, Y., Goldfarb, L., Gomis, M. I., Huang, M., Leitzell, K., Lonnoy, E.,

- Matthews, J. B. R., Maycock, T. K., Waterfield, T., Yelekçi, O., Yu, R., and Zhou, B., Cambridge University Press, 1513–1766, 10.1017/9781009157896.013, 2021.
- 1045 Simmons, A. J., Berrisford, P., Dee, D. P., Hersbach, H., Hirahara, S., and Thepaut, J. N.: A reassessment of temperature variations and trends from global reanalyses and monthly surface climatological datasets, *Quarterly Journal of the Royal Meteorological Society*, 143, 101-119, 10.1002/qj.2949, 2017.
- Stahl, K., Kohn, I., Blauhut, V., Urquijo, J., De Stefano, L., Acacio, V., Dias, S., Stagge, J. H., Tallaksen, L. M., Kampragou, E., Van Loon, A. F., Barker, L. J., Melsen, L. A., Bifulco, C., Musolino, D., de Carli, A., Massarutto, A.,
- 1050 Assimacopoulos, D., and Van Lanen, H. A. J.: Impacts of European drought events: insights from an international database of text-based reports, *Nat Hazard Earth Sys*, 16, 801-819, 10.5194/nhess-16-801-2016, 2016.
- Su, C.-H., Ryu, D., Dorigo, W., Zwieback, S., Gruber, A., Albergel, C., Reichle, R. H., and Wagner, W.: Homogeneity of a global multisatellite soil moisture climate data record, *Geophysical Research Letters*, 43, 11245-11252, 10.1002/2016gl070458, 2016.
- 1055 Teuling, A. J., Van Loon, A. F., Seneviratne, S. I., Lehner, I., Aubinet, M., Heinesch, B., Bernhofer, C., Grunwald, T., Prasse, H., and Spank, U.: Evapotranspiration amplifies European summer drought, *Geophysical Research Letters*, 40, 2071-2075, 10.1002/grl.50495, 2013.
- Trnka, M., Brazdil, R., Mozny, M., Stepanek, P., Dobrovolny, P., Zahradnicek, P., Balek, J., Semeradova, D., Dubrovsky, M., Hlavinka, P., Eitzinger, J., Wardlow, B., Svoboda, M., Hayes, M., and Zalud, Z.: Soil moisture trends in the Czech
- 1060 Republic between 1961 and 2012, *International Journal of Climatology*, 35, 3733-3747, 10.1002/joc.4242, 2015.
- Vreugdenhil, M., Dorigo, W. A., Wagner, W., de Jeu, R. A. M., Hahn, S., and van Marle, M. J. E.: Analyzing the Vegetation Parameterization in the TU-Wien ASCAT Soil Moisture Retrieval, *Ieee Transactions on Geoscience and Remote Sensing*, 54, 3513-3531, 10.1109/Tgrs.2016.2519842, 2016.
- Vroege, W., Bucheli, J., Dalhaus, T., Hirschi, M., and Finger, R.: Insuring crops from space: the potential of satellite-
- 1065 retrieved soil moisture to reduce farmers' drought risk exposure, *European Review of Agricultural Economics*, 48, 266-314, 10.1093/erae/jbab010, 2021.
- Wagner, W., Lemoine, G., and Rott, H.: A method for estimating soil moisture from ERS scatterometer and soil data, *Remote Sensing of Environment*, 70, 191-207, Doi 10.1016/S0034-4257(99)00036-X, 1999.
- Wagner, W., Lindorfer, R., Melzer, T., Hahn, S., Bauer-Marschallinger, B., Morrison, K., Calvet, J. C., Hobbs, S., Quast, R.,
- 1070 Greimeister-Pfeil, I., and Vreugdenhil, M.: Widespread occurrence of anomalous C-band backscatter signals in arid environments caused by subsurface scattering, *Remote Sensing of Environment*, 276, 10.1016/j.rse.2022.113025, 2022.
- Wang, S. S., Mo, X. G., Liu, S. X., Lin, Z. H., and Hu, S.: Validation and trend analysis of ECV soil moisture data on cropland in North China Plain during 1981-2010, *Int J Appl Earth Obs*, 48, 110-121, 10.1016/j.jag.2015.10.010, 2016.
- Wen, J., Wu, X., You, D., Ma, X., Ma, D., Wang, J., and Xiao, Q.: The main inherent uncertainty sources in trend estimation
- 1075 based on satellite remote sensing data, *Theoretical and Applied Climatology*, 151, 915-934, 10.1007/s00704-022-04312-0, 2022.

- WMO: Guidelines on the definition and monitoring of extreme weather and climate events Draft version – first review by TT-DEWCE (Dec 2015), online, https://ane4bf-datapl.s3-eu-west-1.amazonaws.com/wmocms/s3fs-public/event/related_docs/DraftversionoftheGuidelinesontheDefinitionandMonitoringofExtremeWeatherandClimateEvents.pdf, 15-09-2023, 2016.
- 1080 Wouters, H.: Global bioclimatic indicators from 1979 to 2018 derived from reanalysis [dataset], 10.24381/cds.bce175f0, 2021.
- Yang, C. X., Cagnazzo, C., Artale, V., Nardelli, B. B., Buontempo, C., Busatto, J., Caporaso, L., Cesarini, C., Cionni, I., Coll, J., Crezee, B., Cristofanelli, P., de Toma, V., Essa, Y. H., Eyring, V., Fierli, F., Grant, L., Hassler, B., Hirschi, M., 1085 Huybrechts, P., Le Merle, E., Leonelli, F. E., Lin, X., Madonna, F., Mason, E., Massonnet, F., Marcos, M., Marullo, S., Muller, B., Obregon, A., Organelli, E., Palacz, A., Pascual, A., Pisano, A., Putero, D., Rana, A., Sanchez-Roman, A., Seneviratne, S. I., Serva, F., Storto, A., Thiery, W., Throne, P., Van Tricht, L., Verhaegen, Y., Volpe, G., and Santoleri, R.: Independent Quality Assessment of Essential Climate Variables: Lessons Learned from the Copernicus Climate Change Service, *Bulletin of the American Meteorological Society*, 103, E2032-E2049, 10.1175/Bams-D-21-0109.1, 2022.
- 1090 Yang, J., Gong, P., Fu, R., Zhang, M. H., Chen, J. M., Liang, S. L., Xu, B., Shi, J. C., and Dickinson, R.: The role of satellite remote sensing in climate change studies, *Nature Climate Change*, 3, 875-883, 10.1038/Nclimate1908, 2013.
- Zaitchik, B. F., Rodell, M., Biasutti, M., and Seneviratne, S. I.: Wetting and drying trends under climate change, *Nature Water*, 1, 502-513, 10.1038/s44221-023-00073-w, 2023.
- Zheng, X. M., Zhao, K., Ding, Y. L., Jiang, T., Zhang, S. Y., and Jin, M. J.: The spatiotemporal patterns of surface soil 1095 moisture in Northeast China based on remote sensing products, *Journal of Water and Climate Change*, 7, 708-720, 10.2166/wcc.2016.106, 2016.
- Zheng, Y. C., Coxon, G., Woods, R., Power, D., Rico-Ramirez, M. A., McJannet, D., Rosolem, R., Li, J. Z., and Feng, P.: Evaluation of reanalysis soil moisture products using cosmic ray neutron sensor observations across the globe, *Hydrology and Earth System Sciences*, 28, 1999-2022, 10.5194/hess-28-1999-2024, 2024.
- 1100 Zotta, R. M., Moesinger, L., van der Schalie, R., Vreugdenhil, M., Preimesberger, W., Frederikse, T., de Jeu, R., and Dorigo, W.: VODCA v2: Multi-sensor, multi-frequency vegetation optical depth data for long-term canopy dynamics and biomass monitoring, *Earth Syst. Sci. Data Discuss.*, 2024, 1-45, 10.5194/essd-2024-35, 2024.